澳門大學
UNIVERSIDADE DE MACAU
UNIVERSITY OF MACAU

Outstanding Academic Papers by Students

學生優秀作品

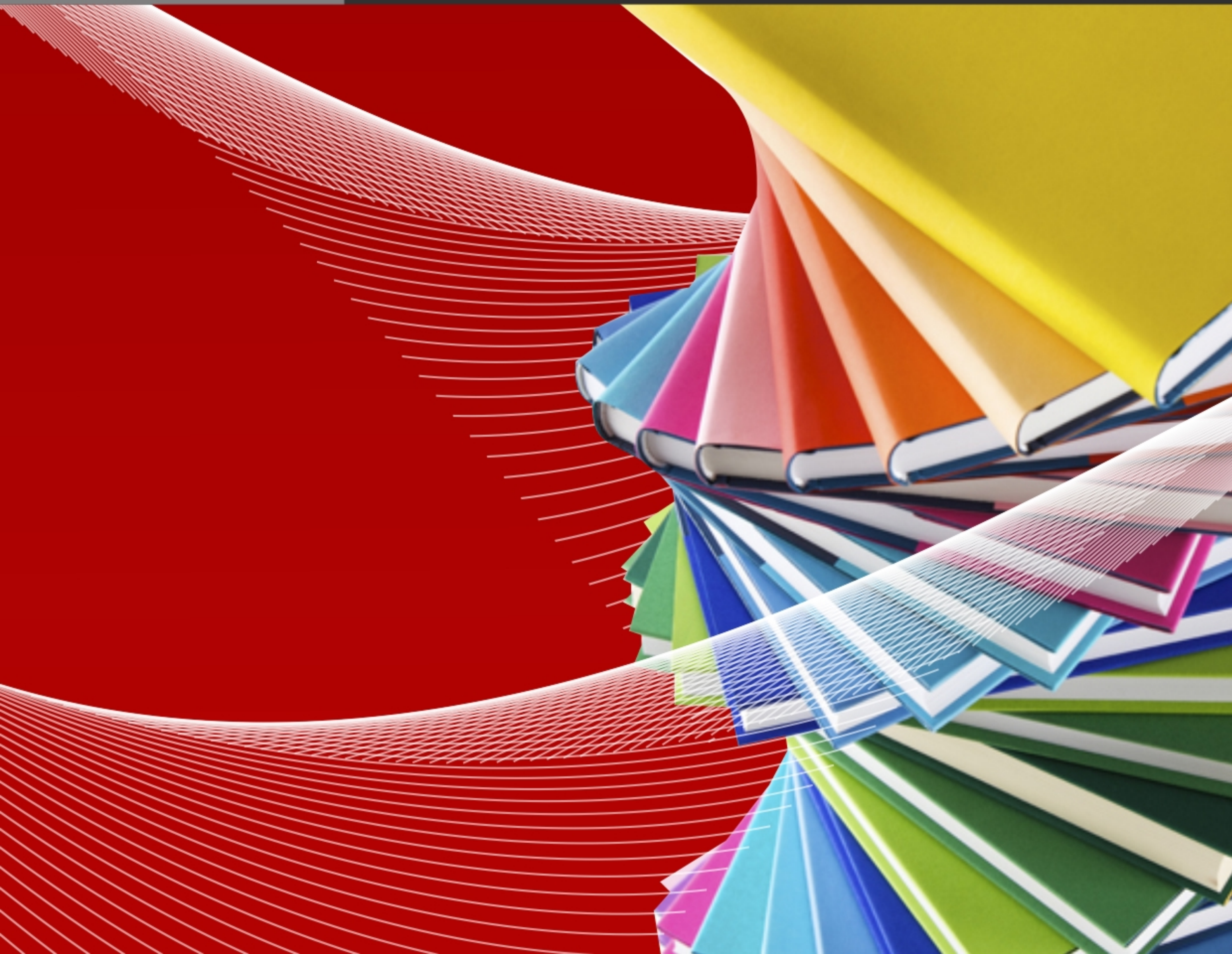

An Exploration of Heart Sound Denoising Method Based on Dynamic Wavelet Shrinkage and Singular Spectrum Analysis

by

ZENG Tao

Final Year Project Report submitted in partial fulfillment
of the requirements for the Degree of

Bachelor of Science in Electrical and Electronics Engineering

2014

Faculty of Science and Technology
University of Macau

********* Bachelor’s Thesis Quote **********

Bachelor’s Thesis (or Final Report of Design Project II)

In presenting this Final Report of Project (ELEC402) in partial fulfillment of the requirements for a Bachelor’s Degree at the University of Macau, I agree that the **UM Library** and **Faculty of Science and Technology (FST)** shall make its copies available strictly for internal circulation or inspection. No part of this thesis can be reproduced by any means (electronic, mechanical, visual, and etc.) before the valid date (usually less than 3 years) limit listed below. Copying of this thesis before the valid date from other parties is allowable **only** under the prior written permission of the author(s).

Printed name: __________________ Signature:______________________

Student number: ________________ Date: _________________________

Reliable Contact information (address, tel. no., email, etc.) of author:

____

____

____

____

Valid date until _________________

********* End of Bachelor’s Thesis Quote **********

University of Macau

Abstract

AN EXPLORATION OF HEART SOUND DENOSING METHOD BASED ON DYNAMIC WAVELET SHRINKAGE AND SINGULAR SPECTRUM ANALYSIS

by ZENG Tao

Thesis Supervisor: Prof. DONG MingChui
Department of Electrical and Electronics Engineering

Intelligent computer-aided heart sound (HS) auscultation provides quantitative and qualitative HS interpretation for preemptive cardiovascular diseases (CVDs). However, the noises corruption in electronic stethoscope acquired HS signals will not only pollute the HS pathological characteristics but also deteriorate diagnosis accuracy dramatically. Therefore, HS denoising plays a pivotal role to get qualified HS signals for further analysis and interpretation.

In this research, a scheme for HS denoising systems adapting dynamic threshold wavelet shrinkage (DTWS) method and singular spectrum analysis (SSA) are proposed. Massive pathological information contained in murmurs is vulnerable to be distorted by applying traditional wavelet shrinkage (TWS) methods. As an improvement of TWS methods, DTWS method further identifies the HS and murmurs information before denoising. Taking advantage of dynamic thresholds, DTWS methods could overcome the shortcomings of TWS method and reserve the foremost HS and murmurs information while eliminating noises utmostly. SSA can efficiently decompose the HS signals with noise into meaningful components representing the constituent of original signals. After reserving the effective eigenvalues, the principal components of HS are picked up and re-assembled as the final de-noised HS.

Experiments using HS signals from eGeneral Medical benchmark database validate the high performance of the proposed denoising scheme adapting DTWS method and SSA in terms of signal-noise ratio (SNR) and root mean square error (RMSE). The results also demonstrated that the proposed denoising scheme not only eliminates the noise components from HS efficiently, but also retains the pathological details of the original HS signals.

TABLE OF CONTENTS

LIST OF FIGURES

Number *Page*

LIST OF TABLES

LIST OF SYMBOLS

A2: Aortic Valve

CVDs: Cardiovascular Diseases

CWT: Continuous Wavelet Transform

DTWS: Dynamic Threshold Wavelet Shrinkage

DWT: Discrete Wavelet Transform

EAS: Early Aortic Stenosis

EHS: Extra Heart Sounds

FFT: Fast Fourier Transform

HS: Heart Sound

IFT: Inverse Fourier Transform

M1: Mitral Valve

MAS: Mild Aortic Stenosis

MRA: Multi-Resolution Analysis

P2: Pulmonary Valve

PCG: Phonocardiogram

PHS: Primary Heart Sounds

RMSE: Root Mean Square Error

S1: First Heart Sound

S2: Second Heart Sound

S3: Third Heart Sound

S4: Fourth Heart Sound

SNR: Signal-Noise Ratio

SSA: Singular Spectrum Analysis

STFT: Short-Time Fourier Transform

SVD: Singular Value Decomposition

T1: Tricuspid Valve

TWS: Traditional Wavelet Shrinkage

WT: Wavelet Transform

ACKNOWLEDGEMENTS

First, I would like to express my gratitude to my supervisor Prof. DONG MingChui for his support and suggestions to my final year project and further planning on my study and research. His guidance helps me to have a deeper understanding of doing research and expressing my idea in presentations and reports.

I also would like to thank my co-supervisor Miss MA JiaLi for her research experience sharing and patient guidance on drafting and formatting my conference papers and final year report. Moreover, I would like to thank other members in our group for their valuable comments and support of my work.

As far as project is concerned, I would like to gratefully acknowledge the support of the Research Committee of University of Macau under Grant No. MYRG184 (Y2-L3)-FST11-DMC and the Science and Technology Development Fund (FDCT) of Macau S.A.R under Grant No. 016/2012/A1.

Finally, I would like to express my sincere appreciation to my parents for their endless love and encouragements during my life.

CHAPTER 1: INTRODUCTION

1.1 RESEARCH BACKGROUND

Cardiovascular diseases (CVDs) are becoming the leading cause of death worldwide nowadays, more people die annually from CVDs than from any other causes. An estimated 17.3 million people died from CVDs in 2008, representing 30% of all global deaths. Among these deaths, an estimated 7.3 million were due to coronary heart disease and 6.2 million were due to stroke. Moreover, the number of people who die from CVDs, mainly from heart disease and stroke, will increase to reach 23.3 million by 2030 [2] [19]. Considering such a grim situation, treatment of CVDs becomes more and more important.

However, CVDs always happen with sudden and unexpected heart attack. Therefore, the pre-diagnosis of CVDs in early stage can reduce the difficulty of treatment and death rate from them correspondingly. Initially, the heart sound (HS) auscultation and analysis of phonocardiogram (PCG) are utilized by physicians for CVDs pre-diagnosis. Recently, with the development of technology, plenty of new diagnostic devices such as echocardiogram [23], photoplethysmogram [11], electrocardiogram [25] are put into use in hospitals. As a result, the significance of HS sound auscultation is diminished. However, the auscultation of heart is still the first basic analysis tool used to evaluate the functional state of the heart [18]. PCG, as the first-hand resource from HS directly, contains tremendous physiological and pathological heart information and makes it potential for early prediction and preemptive diagnosis of CVDs in advance of noticeable symptoms and illnesses. Therefore, it is worthwhile to have HS auscultation as pre-diagnosis of CVDs before any further medical testing.

1.2 INTRODUCATION TO HEART SOUND

1.2.1 HEART STRUCTURE AND HEART SOUND COMPONENTS

Heart is a myogenic muscular organ found in all animals with a circulatory system (including all vertebrates), which pumps blood throughout the blood vessels by repeated, rhythmic contractions. HSs are generated by vibration of the heart values during their opening and closure and by vibration of the myocardium. The associated HS structures can reflect the physiological and pathological characteristics of heart. In early history of CVDs diagnosis, the physical examination is taken as the most common way to evaluate the cardiovascular system. Acoustic information of heart through mechanical stethoscope forms the core of physical examination and diagnosis. Figure 1 shows the physical structure of heart.

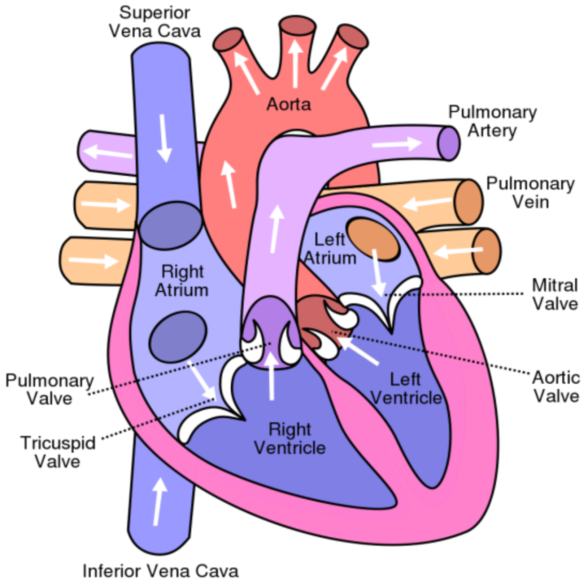

Figure 1: Physical structure of heart

Generally, there are two primary acoustic vibrations sound like “lub” and “lab” occurring in sequence during diastolic and systolic process of heart. They are named as first HS (S1) and second HS (S2) respectively. In addition to these normal sounds, a variety of other sounds may be present including heart murmurs, adventitious sounds, and gallop rhythms third HS (S3) and fourth HS (S4). Figure 2 shows some cardiac cycle examples of HS with different components.

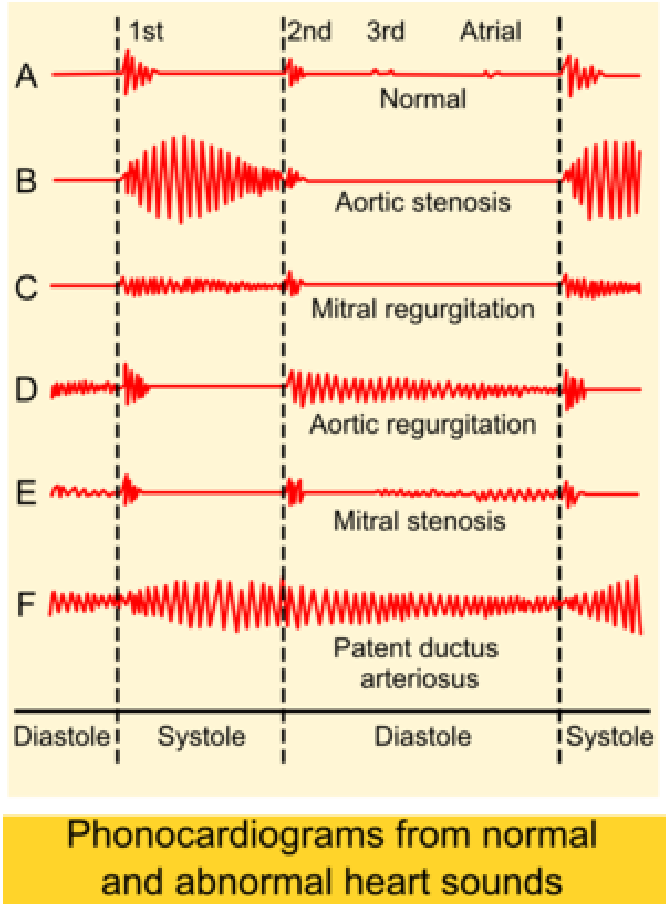

Figure 2: Cardiac cycle examples of HS with different components

All the acoustic information of HS is caused by the following factors [31]: (a) snap and shut of different heart valves; (b) flow of blood through the valve orifice; (c) flow of blood into the ventricular chambers; (d) rubbing of cardiac surface during the heart blood circulation process. The basic flow diagram of blood circulation through heart is shown in Figure 3.

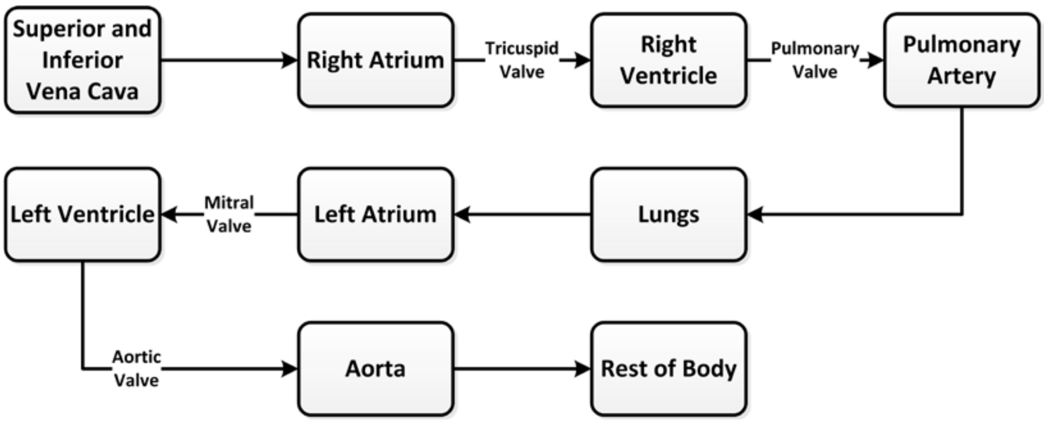

Figure 3: Blood circulation through the heart

S1 includes two components, mitral valve (M1) and tricuspid valve (T1), caused by the closure of mitral valve and tricuspid valve respectively. The components of S2 are due to the closure of the aortic valve (A2) and pulmonary valve (P2) [3]. S3 occurs at the beginning of diastole after S2 and is lower in pitch than S1 or S2 as it is not of valvular origin. It is benign in youth, some trained athletes, and sometimes in pregnancy. S4 when audible in an adult is called a pre-systolic gallop or atrial gallop. This gallop is produced by the sound of blood being forced into a stiff or hypertrophic ventricle. S1 and S2 are normal HSs associated with heart valves closing, causing changes in blood flow. Therefore, they also classified as primary heart sounds (PHS). S3 and S4 could be heard in both normal and abnormal situations and both of them are rare in HS auscultation, thus they are summarized as extra heart sounds (EHS).

Heart murmurs are produced by turbulence of blood, which may occur inside and outside the heart. In details, there are five main factors involved in the production of murmurs [28]: (a) high rates of flow through the valves; (b) flow through a constricted valve (stenosis); (c) backward flow through an incompetent valve (insufficiency or regurgitation); (d) abnormal shunts between the left and right side of the heart (septal defects); (e) Decreased viscosity, which causes increased turbulence.

Heart murmurs may be pathological (abnormal) and physiological (benign). Abnormal murmurs can be caused by stenosis restricting the opening of a heart valve, resulting in turbulence as blood flows through it. Abnormal murmurs may also occur with valvular insufficiency (regurgitation), which allows backflow of blood when the incompetent valve closes with only partial effectiveness. Different murmurs are audible in different parts of the cardiac cycle, depending on the cause of murmurs.

1.2.2 Heart Sound Auscultation

The technique of listening to HSs, called auscultation, has been used for diagnostic purpose since the 16th century. With hundreds of years' development, mechanical stethoscope was invented and widely used in auscultation of circulatory and respiratory systems. However, auscultation of HS using the traditional mechanical stethoscope with human ear depends on substantial clinical experience of doctors. Moreover, the human ear is not very well suited to recognize the several events of short duration occurring in small intervals of time, especially in the low-frequency range as shown in the Figure 4. The HS signal frequency band locates from 20 to 1000 Hz, which is overlapped with different kinds of noised in frequency domain. Moreover, the audibility of human ears only covers a part of HS signal in frequency-intensity domain. As a consequence, the diagnostic accuracy is restricted.

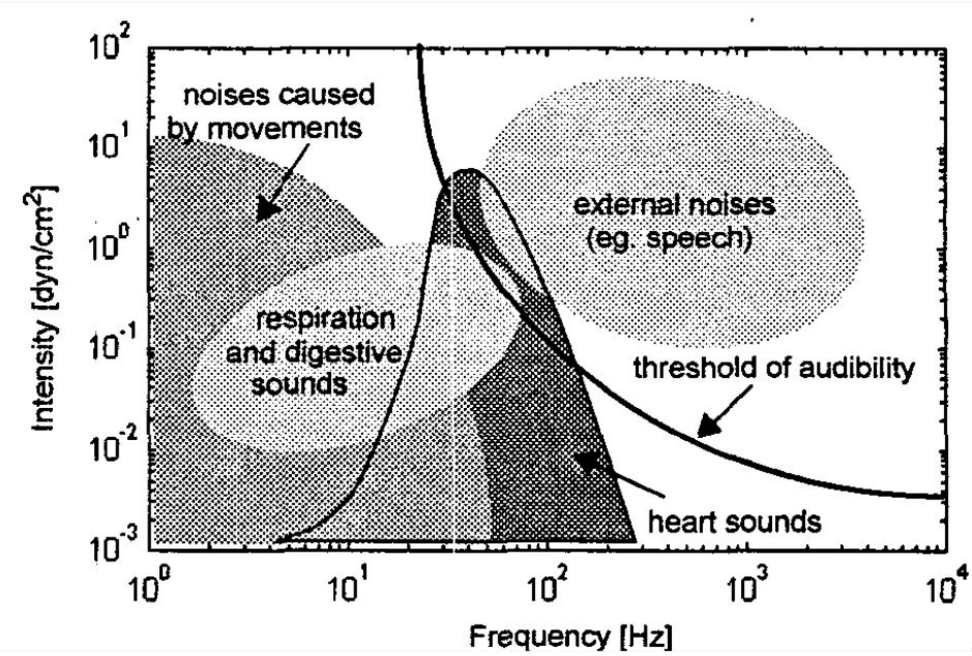

Figure 4: Spectral intensity map of phonocardiograph records

The emergence of electronic stethoscope overcame the drawbacks of the traditional mechanical stethoscope. By placing an electronic stethoscope against human chest skin, computer-aided HS auscultation and diagnosis provide an efficient way for qualitative and quantitative HS analysis. In addition to the basic auscultation, it allows the detection of sub-audible sounds and murmurs and makes a permanent record of these events by converting acoustic wave into electrical signals which can then be amplified and processed for optimal listening. Furthermore, it exhibits several advantageous features over traditional HS auscultation paradigm: (a) free from inherent human ears limitation; (b) high efficient to deal with vast amount of HS signals simultaneously; (c) high precise by considering both audible and inaudible HS components during diagnosis; (d) capable to record, replay, and store HS signals efficiently. Since cardiac disorders can be detected effectively and efficiently in HS auscultation, the intelligent analysis techniques of HS signals play an important role in clinical CVDs diagnosis.

There are four important areas used for listening to HSs. They are aortic area (right second intercostal space), pulmonic area (left second intercostal space), tricuspid area (mid-left sternal border), and mitral area (fifth intercostal space, midclavicular line). The location of auscultatory sites and valves (P, A, T and M) are shown in Figure 5. As mentioned previously, the closure of M1 and T1 caused S1 and the closure of A2 and P2 generated S2. Combining to the auscultatory sites, both the first and second sounds can be heard at all sites, but some pathologic and normal sounds are heard best at one site or another. M is best heard over the apex of the heart at mitral area, and T is best heard over the mid-left sternal border at tricuspid area. A is best heard at the aortic area (right second intercostal space), and P is best heard at the pulmonic area (left second intercostal space).

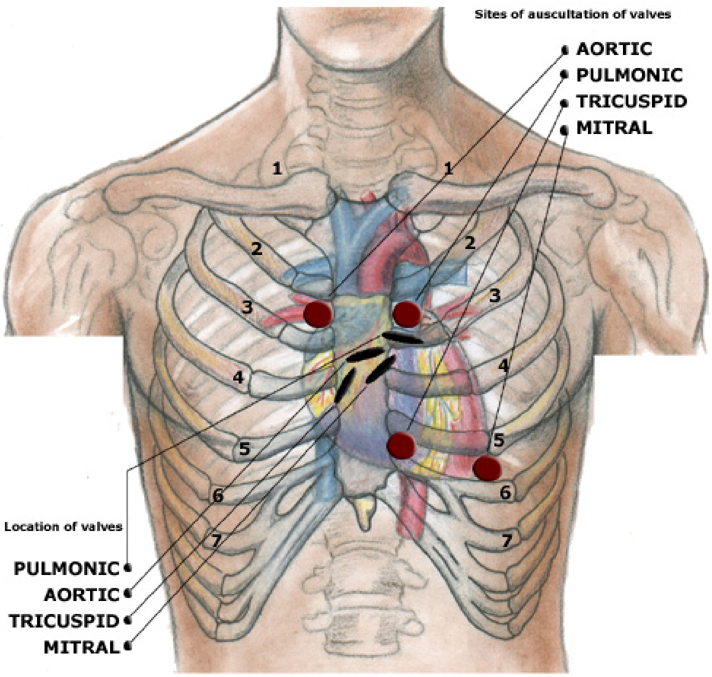

Figure 5: The location of auscultatory sites and valves

1.2.3 HEART SOUND NOISES

The modern technologies make it much more convenient for HS auscultation. Utilizing electronic stethoscopes to record HS signals, intelligent data analysis algorithms can help to realize further analysis and diagnosis. However, the acquired HS signals from electronic stethoscopes suffer a lot from diversified noises corruption by sounds of lung and breathe, contact of electronic stethoscope with skin, environmental noises, and other ambient sounds randomly. These noises will not only pollute the HS pathological characteristics but also deteriorate diagnosis accuracy dramatically. What's more, the various noise components make the diagnostic evaluation of HS records difficult or even impossible [29]. HS noises can be briefly divided into three types: (a) Internal body noises, (b) External body noises, and (c) System noises. Internal body noises are created inside the human body. For example, respiratory sounds come from lung and acoustic damping through the bones and tissues. The sources of these noises are close to HS and easy to mix with each other. External body noises are noises generated outside human body, such as environmental noise and shear noises from the friction of stethoscope head and skin. Since HS is weak, the external noises have a great impact on the components of HS signal, which may even directly cover useful information for HS analysis and diagnosis. System noises are unavoidable when we use electronic instruments for HS auscultation. For instance, Gaussian white noise, baseline-drift noise and power line noise always exist during HS auscultation.

In practical cases, the key noises affecting further HS analysis can be classified into two categories according to their distribution in time domain. One is the stationary noise, such as white noise with a constant power spectral density. The other is the irregular noise, such as environmental noises exist during HS signal acquisition. Therefore, HS denoising plays a pivotal role to obtain the qualified HS signals for further analysis and interpretation. With a dedicated HS denoising system, the intelligent HS interpretation and diagnosis in e-home healthcare platform will then become realizable.

1.3 LITERATURE REVIEW

There are plenty of literatures on HS denoising according to the previous research work. Before 21st century, researchers usually applied digital band-pass filters (most commonly IN-filters of FET-based filtering) as a simple denoising method [5]. The cut-off frequencies of the filters are determined by empirical observations. Although band-pass filtering removes a relevant part of the disturbances, it has also impact on the useful HS information which also overlaps in the filtered frequency bands.

At the beginning of 21st century, more and more researchers realized the overlapping problem and tried to explore new analysis methods beyond the frequency-domain information. From recent years, there are mainly three most common methods: wavelet threshold [9], adaptive filter [13], and mathematical morphology [10]. The wavelet and its derivative algorithms are most widely applied on HS denoising. With the aid of spatially adaptive technique and shrinkage of empirical wavelet coefficients, the wavelet shrinkage methods are able to choose wavelet reconstructions selectively and adaptively to realize efficient noise reduction [20]. In order to obtain higher denoising performance, several adjustments on shrinkage threshold functions have been made [34] [32] based on the traditional wavelet shrinkage (TWS) method. In [34], the generalized threshold function adapted the Stein Unbiased Risk Estimate is employed whereas [32] improves the hard and soft thresholds by inducing two parameters to control the smoothness of signal denoising and adjust the constant deviation between threshold and the original wavelet coefficients correspondingly. However, traditional wavelet threshold shrinkage method is difficult to extract the low-frequency noise and may loss the useful information of HS signals in high-frequency range [30]. For instance, the murmurs which contain pathological information are usually overlapped with noises in high-frequency domain [17]. For the adaptive filter and mathematical morphology method, the priori information of noise and HS signal is required, which is not achievable to in practical CVDs diagnosis without large empirical databases.

1.4 BOTTLE-NECK PROBLEMS

As a summary of the HS signal denoising background, it can be found that plenty of previous works related to HS denoising utilize stationary white noise as the noise model to verify and evaluate HS denoising performance. However, in practical applications, various noises are mixed with HS signals during acquisition, among which irregular noise (e.g. environmental noise) is a common noise source but has never be exploited. Therefore, using ideal normal heart sound from database with stationary noise model to evaluate the denoising performance is not comprehensive and rigorous.

Moreover, most of the HS denoising methods utilize murmur-free HS signals as the testing signal to verify the denoising performance. Despite the reported high denoising performance for normal murmur-free HS signals, those methods are not for pathological HS signals with murmurs in practical diagnosis. Since murmurs reflect massive pathological information and exhibit comparable amplitudes with noises, a direct application of TWS method on HS signals with murmurs will result in loss of pathological information by mistaking murmurs as noises during denoising process. Therefore, how to make a delicate trade-off between eliminating noises and keeping pathological information simultaneously when tackling HS signals with murmurs is also one of bottleneck problems.

1.5 RESEARCH GOALS

The qualified HS signals are important and necessary for further analysis and diagnosis. However, during the acquisition of HS signal, there are diversified noises mixed with the HS signal and make the original HS signal difficult to be analyzed directly. The confliction between the demand of qualified HS signal to the HS analysis system and supply of the polluted HS signal obtained from the HS acquisition system lead to the scheme design of the HS denoising system as proposed in this thesis. The research goals can be concluded in detail as follows:

(a) Develop a new method to eliminate stationary noises and retain pathological information simultaneously.

(b) Adapt time-series analysis methods on HS denoising to eliminate irregular noises during the HS acquisition.

(c) Construct a testing environment to verify and evaluate the performance of HS denoising methods using HS signal samples from benchmark databases.

In summary, the ideal HS denoising system is supposed to be able to eliminate both stationary and irregular noise components and retain the fidelity of HS pathological information. Hence it is able to provide qualified HS signals for further HS analysis and diagnosis as a part of e-home healthcare system.

1.6 DISSERTATION OVERVIEW

This thesis consists of seven chapters. The research background and literature review is introduced in this chapter. After reviewing the development of HS auscultation and denoising techniques, the bottle-neck problems hampering further HS analysis and diagnosis in e-home healthcare system are pointed out. The corresponding research goals are illustrated. In Chapter 2, an overview of time-frequency analysis shows the superiority of wavelet transform (WT) in time-frequency analysis and the framework of SSA are represented. Chapter 3 briefly introduces the preprocessing part of the system as the first denoising step. Chapter 4 presents DTWS method as an improvement of the traditional wavelet shrinkage method to remove stationary noises by time-frequency analysis. Chapter 5 further describes the detail steps of SSA. Chapter 6 shows the representative results of the proposed HS signal denoising system with signal-noise ratio (SNR) and root mean square error (RMSE) as HS denoising performance evaluations. The conclusion and further improvement are drawn in Chapter 7.

CHAPTER 2: RELEVANT THEORIES

The time-frequency analysis is the core part of HS signal processing. For HS denoising, the main purpose is to separate the invalid noise component away from original HS signal sound to obtain the qualified signal for further HS analysis and diagnosis. The time and frequency characteristic differences between HS signal components and noise components are the criterion for HS denoising.

2.1 Fourier Transform

Fourier transform (FT) is a method of analysis that was developed by Jean B. Joseph Fourier in 1807. It plays an important part in the signal processing [26]. In 1976 Ajit P. Yoganathan et al. used fast Fourier transform (FFT) to analysis the S1s from 29 normal healthy young males, which introduced FT into HS analysis firstly [33]. The FT that is used to determine the frequency constituent of the raw signal in the time domain can be defined with the two equations as follows by Eq. (1) and (2):

$$X(\omega) = \int_{-\infty}^{\infty} x(t) e^{-j\omega t} dt \tag{1}$$

$$x(t) = \frac{1}{2\pi} \int_{-\infty}^{\infty} X(\omega) e^{j\omega t} d\omega \tag{2}$$

where t represents time, ω indicates angular frequency, x specifies the signal in the time domain and $X(\omega)$ specifies the signal in the frequency domain. In the Eq. (1) and (2) given above, the FT of $x(t)$ and the inverse Fourier transform (IFT) are displayed.

Although FT is widely used in signal analysis, there is a drawback that cannot be ignored. The FT can represent the components distribution in frequency domain, but it completely loses the time-domain information of the signal to be transformed. For stationary signals without time-varying characteristic, the drawback is not that obvious. However, for non-stationary signals such as HS signal, the characteristics in time domain are non-negligible. FT does not provide enough information in-time domain, thus it fails to apply on HS denoising.

2.2 Short-Time Fourier Transform

Short-time Fourier Transform (STFT) is a Fourier-related transform used to determine the sinusoidal frequency and phase content of local sections of a signal as it changes over time. It overcomes the drawback of FT which missing time-domain information. It can be used for analyzing non-stationary signals, whose statistic characteristics vary with time. In essence, STFT extracts several frames by windows of the signal to be analyzed with a window that moves with time based on FT. The location of the sliding windows indicates the time-domain characteristic. Combining with the frequency domain characteristics, the time-frequency analysis can be achieved. At the beginning of 21th century, the STFT is applied to a normal PCG signal in order to characteristic HS (S1 and S2) components in both time and frequency domain [7]. It can be expressed in Eq. (3):

$$X(\tau,\omega) = \int x(\tau)\omega(t-\tau)dt \tag{3}$$

where $\omega(t)$ is the window function, $x(t)$ represents the signal to be transformed. The time index τ is normally considered to be "slow" time and usually not expressed in as high resolution as time t.

STFT is an effective method to make up the drawbacks of FT, which provides the time and frequency information simultaneously. However, the window size of STFT is fixed and the precision is restricted. In details, due to the "window effect" of STFT, the window size in both low and high frequency range is same to each other, which means the resolution in higher and lower frequency domain is different between each other. This property limits the application of STFT in high-resolution and large-band frequency signal analysis. Therefore, STFT is suitable to analysis qualified HS after denoising but not fairish enough for HS denoising.

2.3 Wavelet Transform

The wavelet transform (WT) was developed as a method to obtain simultaneous, high resolution time and frequency in formation about a signal. The term 'wavelet' was first mentioned in 1909 in a thesis by Alfred Haar [22], although the progress in the field of wavelets has been relatively slow until the 1980s when the scientists and engineers from different field realized they were working on the same concept and began collaborating. [16]

The WT presents an improvement over the STFT because it obtains good time-frequency resolution by using a flexible sized region (the wavelet) instead of a constant window size in STFT. While a narrow wavelet extracts high frequency components, a stretched wavelet picks up on the lower frequency components of the signal.

A wavelet is a signal if limited duration that has an average value of zero. The mathematical description of Continuous Wavelet Transform (CWT) is described by Eq. (4).

$$CWT_x^{\psi}(\tau, s) = \Psi_x^{\psi}(\tau, x) = \frac{1}{\sqrt{|s|}} \int x(t) \psi^* \left(\frac{t-\tau}{s} \right) dt \tag{4}$$

where ψ is the mother wavelet function, x is the signal to be transformed, τ is the shift factor and the scale factor s of the wavelet may conceptually be considered the inverse of frequency. The CWT reveals more detail about a signal, but since all scales are used to compute the WT, the computation time can be enormous. Therefore, the discrete wavelet transform (DWT) is more widely used. The DWT calculates wavelet coefficients at discrete intervals of time and scale, instead of at all scales. The DWT requires much less computation time than the CWT without much loss in detail. In practical applications, parameters s and τ of mother wavelet function ψ are converted to discrete form, which can be expressed by Eq. (5):

$$\psi_{j,k}(t) = 2^{j/2} \psi(2^j t - k) \tag{5}$$

The corresponding DWT is defined in Eq. (6):

$$DWT_x^{\psi}(j,k) = \int_{-\infty}^{\infty} x(t) \psi^*{}_{j,k}(t) dt \tag{6}$$

Discrete wavelet $\psi_{j,k}(t)$ is a function family converted from $\psi(t)$ by zooming of 2^j times and shifting k units. Which means the localization of time and frequency can be adjusted by parameter k and j respectively.

With the perfect time-frequency characteristic, WT is widely applied into the non-stationary signal analysis, the time-frequency characteristic comparison between the methods mentioned previously are shown in Figure 6 as follows:

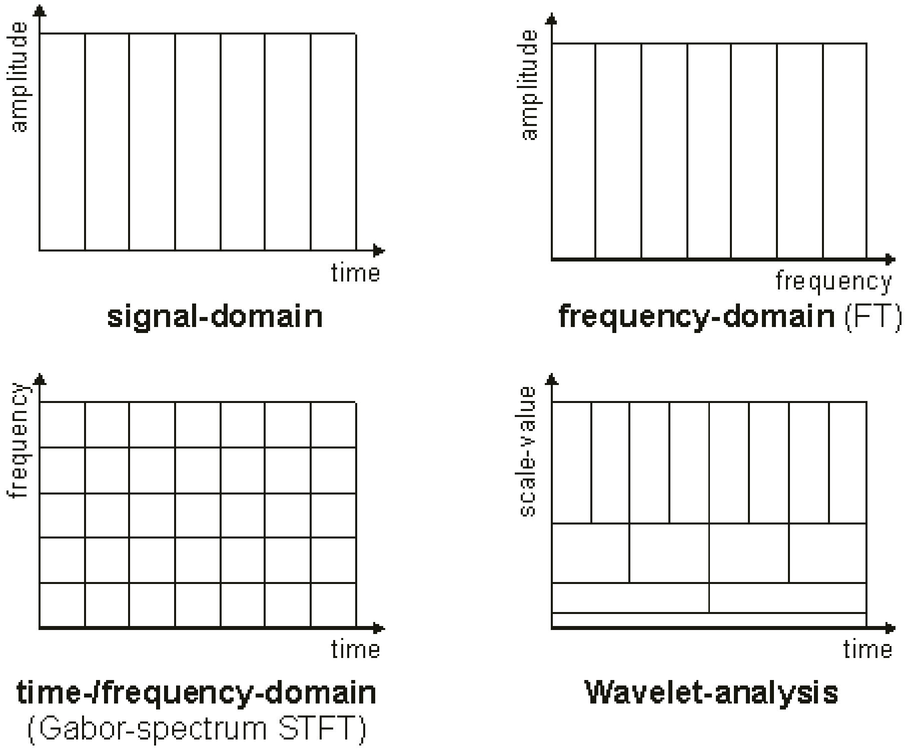

Figure 6: Comparison of time-frequency characteristics

It can be found that WT has multi-resolution characteristic: in larger scale with higher frequency, the time scale is narrower and in smaller scale with lower frequency, the time scale is wider to balance the resolution in different scales. Therefore, utilizing WT denotes higher ability to analysis non-stationary signals (e.g. HS signal) in time-frequency domain.

2.4 Singular Spectrum Analysis

2.4.1 Introduction to Singular Spectrum Analysis

Singular spectrum analysis (SSA), as a nonparametric spectral estimation method in time series analysis, has been adapted to the changes in the statistical properties of the data and effectively used for detection of murmur from HS signals. The basic SSA method consists of two complementary stages: decomposition and reconstruction; 20called time series) is decomposed and in the second stage the original source signal is reconstructed and used for further analysis. The main concept in studying the properties of SSA is separability, which characterizes how well different components can be separated from each other [24]. Generally, there are two advantages of SSA in HS analysis: (a) No phase shift comparing to the traditional filter and (b) Prior information of noise is unnecessary comparing to the adaptive filter. Therefore, SSA is suitable as an algorithm on HS denoising.

2.4.2 SINGULAR VALUE DECOMPOSITION

This stage includes an embedding operation followed by singular value decomposition (SVD). It is assumed that signal sequence **X** is the HS signal after sampling with N points. If the embedding dimension is l and time delay is t, according to Takens' theorem [27], it can be mapped into the $l \times k$ matrix by Eq. (7).

$$\mathbf{X} = \left[x_1, x_2, ..., x_N \right] = \begin{pmatrix} f_0 & \cdots & f_{k-1} \\ \vdots & \ddots & \vdots \\ f_{l-1} & \cdots & f_{r-1} \end{pmatrix} \tag{7}$$

With vectors: $x_i = \left[f_{i-1}, f_i, ..., f_{i+l-2} \right]^T \in R^L$, where $k = r - l + t$ is the window length of the signal sequence ($1 \leq l \leq$ r). The window length is supposed to be sufficiently large but not too large considering of calculation complexity. Actually the minimum value of embedding dimension l of the signal time sequence can be approximately determined by the “Cao’s Method” [4]. Note that the trajectory matrix **X** is a Trajectory matrix, which means that all the elements along the diagonal are equal.

In the SVD stage the SVD of the trajectory matrix is computed and represented as a sum of rank-one bi-orthogonal elementary matrices. Consider the eigenvalues of the covariance matrix expressed by Eq. (8):

$$C = \frac{XX^T}{l} \tag{8}$$

where subscript T denotes the transpose of a vector. Applying SVD to the covariance matrix, it can get a group of non-negative eigenvalues $\{\mathrm{e}_i\}, (i = 1, 2, ..., l)$. Rearrange them in decreasing order of magnitude $(\mathrm{e}_1 \geq \mathrm{e}_2 \geq ... \geq \mathrm{e}_l \geq 0)$, which corresponding to the relative relationships between different components in the signal sequence. The eigenvector **E** is defined as $\mathbf{E} = \{e_1, e_2, \ldots\ldots, e_l\}$. The eigenvalues with relative large magnitude corresponds to principle component (PC) of HS signals and the eigenvalues with relative small magnitude corresponds to noise component. It is also regarded as the determine conditions to do another SVD or to reconstruct the signal at this stage.

CHAPTER 3: SIGNAL PREPROCESSING

Before applying the denoising algorithms, preprocessing should be conducted on the acquired HS signals. Afterwards, the preprocessed HS signals can be further de-noised using the proposed HS denoising algorithms. The preprocessing can be divided into three parts as shown in Figure 7.

Figure 7: The scheme of preprocessing

In the detrending step, the mean value and best fit of the original HS signal are calculated and removed. These float and trend items usually contain disturbances during HS signal acquisition. A FIR digital band-pass filter is designed to remove the noise signal out of the HS signal frequency band between 20 to 1000 Hz. The normalization step sets a series restriction condition to minimize the impact of the physiological factors, which normalizes the amplitude of HS signals from different sources to provide standardized criteria for further analysis.

3.1 Detrending

During HS acquisition, some instrumental noises are introduced, such as periodic baseline drift, DC offset, etc. In order to remove these slowly varying trend items which may superimpose to a fluctuating process to disturb further time-frequency analysis, it is necessary to process the acquired HS signal by removing the mean value and best fit of the signal sequence before carrying further denoising process. An example of detrending results of a signal with trend and float items is shown in Figure 8 as follows.

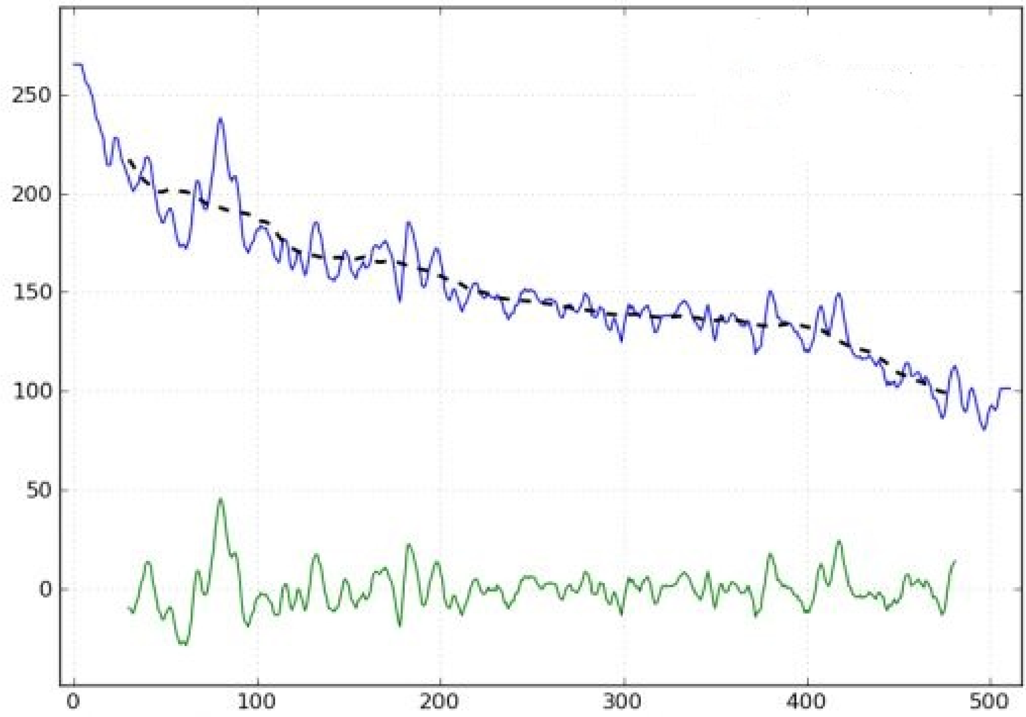

Figure 8: Detrending result of a signal with trend and float items

The blue solid line represents the original signal with trend and float items and the green one is the signal after detrending. The dash line indicates the best fit of the original signal sequence. It can be found that the trend and float items are removed after detrending. Detrending process keeps the characteristic of the original signal and moves some irrelevant fluctuating items at the first stage.

3.2 Band-Pass Filtering

Since the frequencies of HS components locate from 20 to 1000 Hz, a band-pass filter is usually utilized to filter out unnecessary components beyond the HS frequency band. In this case, "fdatool" in Matlab is utilized to design the band-pass filter. The basic design structure of band-pass filter is shown in Figure 9.

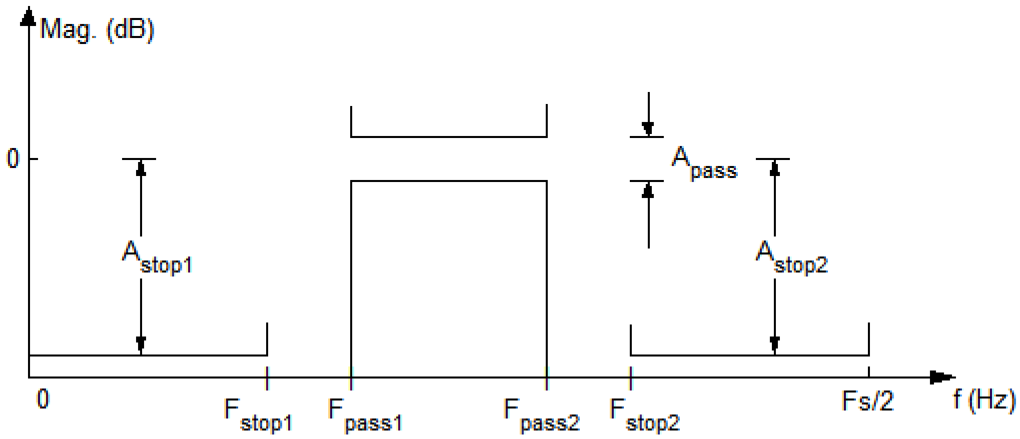

Figure 9: The basic design structure of band-pass filter

The corresponding design parameters of the FIR filter is shown in Table I as follows.

TABLE I: FILTER DESIGN PARAMETERS

Design Method	FIR (Kaiser window)	
Filter Order (N+1)	Minimum order (726)	
Frequency Specifications (Hz)	fs	4000
	F_{stop1}	10
	F_{pass1}	30
	F_{pass2}	900
	F_{stop2}	1100
Magnitude Specifications	A_{stop1}	60
	A_{pass}	1
	A_{stop2}	60

The HS signals from eGeneral Medical benchmark database are employed with sampling frequency of 4000 Hz. Design method is chosen as FIR with Kaiser window. Comparing to IIR filters, FIR filters can achieve linear phase response that process signals without phase distortion. Moreover, they are much easier to implement than IIR filters. Kaiser window has an extra ripple control parameter β to control the relationship between transition widths and pass band ripple as shown in Eq. (9), where A is stop attenuations of magnitude specifications satisfy A = 60 dB in the design. Then the minimum order of the FIR filter can be calculated by Eq. (10).

$$\begin{cases} \beta = 0 & \text{if } A \le 21\,\text{dB} \\ \beta = 0.5842(A-21)^{0.4} + 0.07886(A-21) & \text{if } 21\,\text{dB} < A < 50\,\text{dB} \\ \beta = 0.1102(A-8.7) & \text{if } A \ge 50\,\text{dB} \end{cases} \qquad (9)$$

$$N \geq \frac{A - 7.95}{14.36 \Delta f} \tag{10}$$

where Δf is the normalized transition width. The minimum order is evaluated to be 726 as shown in Table I. The magnitude response of the designed FIR band-pass filter is shown in Figure 10.

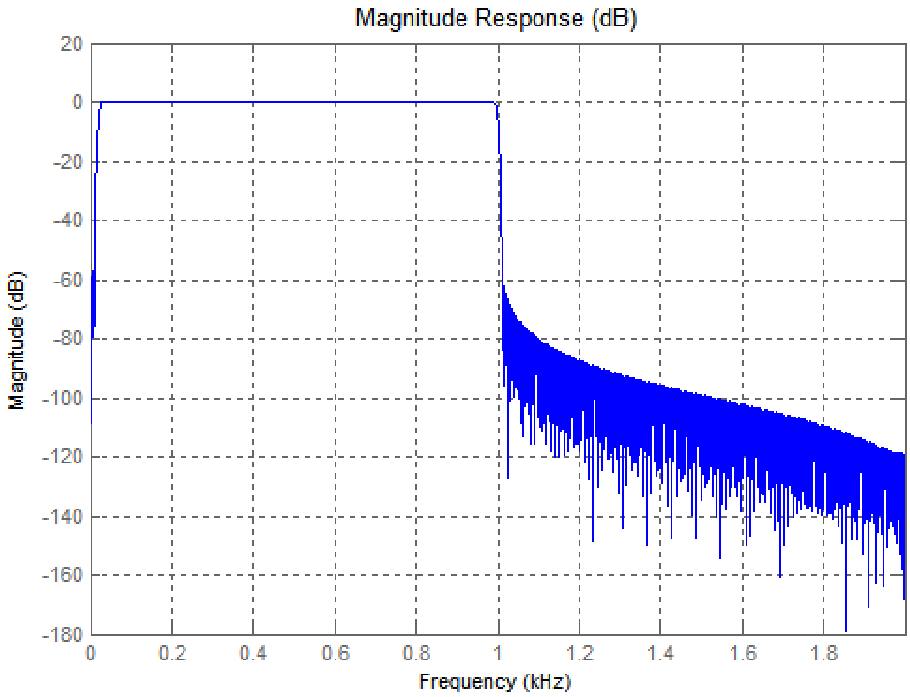

Figure 10: The magnitude response of the designed FIR band-pass filter

3.3 Normalization

Normalization is a basic statistical operation. It is used to scale heterogeneous sets of data, so that they could be compared relevantly. The physiological attributes of HS signals have to be fixed to reduce the impact to the similarity results and make the action of pathological attributes more obviously, so the normalization work must be extremely necessary. In the preprocessing part, normalization helps to regulate the amplitude of HS signals from -1 to +1 as defined in Eq. (11):

$$s_{norm}(n) = \frac{s(n)}{|\max(s(n))|} \tag{11}$$

where $s(n)$ is the original HS signal and $s_{norm}(n)$ is the normalized signal. The normalization is a necessary step for the further time-frequency analysis of HS signal.

CHAPTER 4: DYNAMIC THRESHOLD WAVELET SHRINKAGE METHOD

WT provides a perfect time-frequency analysis platform for HS signals. Based on the idea of WT, TWS method [8] was raised as a signal denoising technique based on the principle of shrinking the wavelet coefficients. It works well to remove stationary white noise. However, TWS method may also remove the murmurs together with noise from the original HS signal at the same time. In this chapter, a novel an dynamic threshold wavelet shrinkage (DTWS) method is proposed adapting TWS method.

Differ from the traditional wavelet shrinkage method, in DTWS the decomposition layers which contain most HS and murmurs information are found out first as characteristic layers. Then dynamic thresholds and traditional shrinkage thresholds are applied on wavelet coefficients of characteristic layers and non-characteristic layers respectively. Finally, the reconstructed HS signal is obtained with noises eliminated greatly. Taking advantage of dynamic thresholds, DTWS could overcome the shortcomings of TWS method and reserve the foremost HS and murmurs information while removing noises utmostly.

The scheme of DTWS method is consisted of decomposition, dynamic wavelet threshold, and reconstruction as shown in Figure 11.

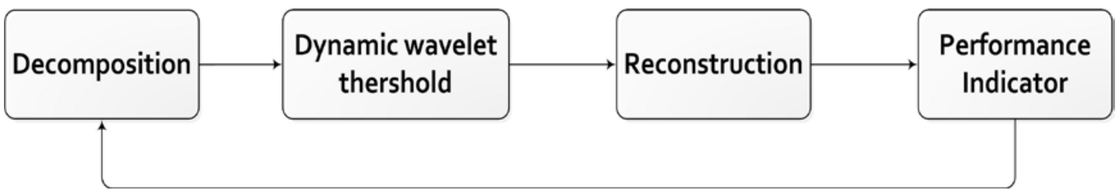

Figure 11: The scheme of DTWS method

Compared with TWS method, the criteria of the threshold setting gets improved in DTWS. After reconstruction, there is a performance indicator to evaluate the denoising performance and feedback the performance indictor value to the decomposition step. As a consequence, the optimal decomposition level can be determined after obtaining the optimal value of performance indicators.

4.1 Multi-Resolution Analysis

The DTWS method is based on DWT which calculates the wavelet coefficients at discrete time and scale intervals. These wavelet coefficients form a set of features for unambiguously characterization of miscellaneous signals [1].

The basic idea of multi-resolution analysis (MRA) is to utilize the multi-scale characteristic of the orthogonal wavelet basis function and expand the signal at different scales for further time-frequency domain analysis. In order to illustrate the principle of multi-resolution, a function space $\{\mathbf{V}_j\}, j \in Z$ is defined as a sub-space of $\mathbf{L}^2(R)$, if they satisfied the properties as follows, then $\{\mathbf{V}_j\}, j \in Z$ is called the MRA of $\mathbf{L}^2(R)$.

(a) If $\forall j \in Z$, then $V_j \supset V_{j+1}$;

(b) $\bigcup_{j \in Z} \mathbf{V}_j = \mathbf{L}^2(R)$; $\bigcap_{j \in Z} \mathbf{V}_j = \{0\}$;

(c) $\forall j \in Z$, if $f(t) \in \mathbf{V}_j$, then $f(2t) \in \mathbf{V}_{j-1}$;

(d) $\forall (j,k) \in Z$, if $f(t) \in \mathbf{V}_j$, then $f(t-k) \in \mathbf{V}_j$;

(e) If $\forall j \in Z$, then $\mathbf{V}_{j+1} = \mathbf{V}_j \oplus \mathbf{W}_j$, where **W** is wavelet function space, **V** and **W** are orthogonal with each other.

(f) There exists a function $\phi \in V_0$ make the set $\{\phi_{0,k} = \phi(-k), k \in Z\}$ constitutes an orthonormal basis for V_0, the set is also called Riesz basis.

The properties above provide possible ways for HS signal analysis and denoising. According to (a), (b), (c) and (d), it can be utilized to recognize the global and local relationships of HS signals in different scale levels. The orthogonality represented by (e) is important in HS analysis and diagnosis. Since the vector spaces **V** and **W** is independent according to the orthogonality, which means there is no redundancy in the different frequency bands. Property (f) shows that all functions in $\mathbf{L}^2(R)$ can be represent by the linear combinations of function ϕ, which is helpful to HS feature extraction.

4.2 Mallat Algorithm

MRA provides a platform to local information analysis of non-stationary signals. In order to process the low-frequency and high-frequency components respectively, Mallat algorithm was proposed as a fast wavelet decomposition and reconstruction method.

Assume a_n^j and d_n^j are the scale coefficient and wavelet coefficient at resolution level j and decomposition layer n in MRA, g_k and h_k are filters which satisfy two-scale difference equation, then a_n^j and d_n^j have the relationship as follows:

$$a_n^j = \sum_{k=-\infty}^{\infty} h_{k-2n} a_k^{j-1} \tag{12}$$

$$d_n^j = \sum_{-\infty}^{\infty} g_{k-2n} a_k^{j-1} \tag{13}$$

Let $\overline{h_n} = h_{-n}$, $\overline{g_n} = g_{-n}$, then the equations above change to:

$$a_n^j = \sum_{k=-\infty}^{\infty} \overline{h_{2n-k}} a_k^{j-1} \tag{14}$$

$$d_n^j = \sum_{-\infty}^{\infty} \overline{g_{2n-k}} a_k^{j-1} \tag{15}$$

Eq. (14) and Eq. (15) are the Mallat algorithm of wavelet decomposition. The schematic diagram of Mallat decomposition is shown in Figure 12 as follows:

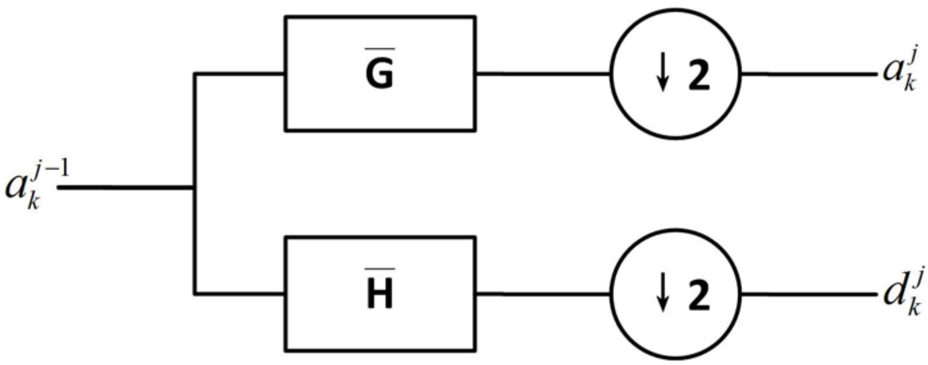

Figure 12: The schematic diagram of Mallat decomposition

where $\overline{\mathrm{G}}$ and $\overline{\mathrm{H}}$ represent the impulse responses of low-pass and high-pass filter respectively. $\downarrow 2$ is the half sampling, which means keep one sample out of two. At each decomposition level, the half-band filters generate signals with half of the original frequency band. As the output signals only remain half band width of the original sampling rate, there is no loss of signal information.

Based on the Mallat algorithm of wavelet decomposition, the Mallat algorithm of wavelet reconstruction can be express as follows in Eq. (16):

$$a_n^{j-1} = \sum_{k=-\infty}^{\infty} h_{n-2k} a_k^j + \sum_{k=-\infty}^{\infty} g_{n-2k} d_k^j \tag{16}$$

The schematic diagram of Mallat reconstruction is shown in Figure 13 as follows:

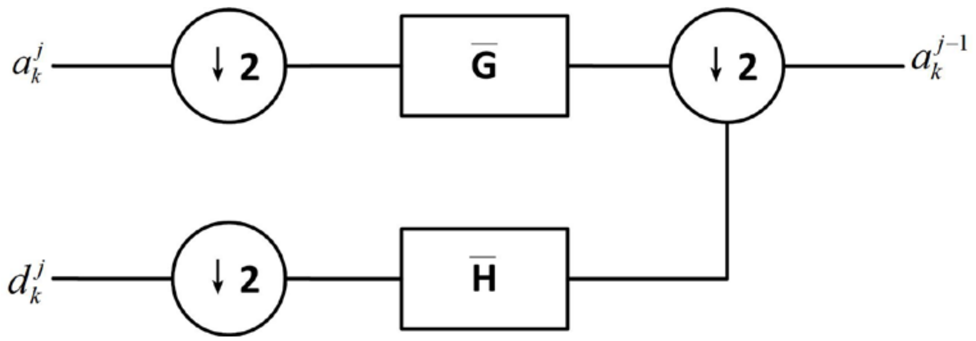

Figure 13: The schematic diagram of Mallat reconstruction

In this case, from a_k^j and d_k^j to a_k^{j-1}, the sampling points doubled as an inverse process of decomposition.

In summary, a signal $x(t)$ in space V_0 is decomposed and reconstructed in Eq. (17) with level of three:

$$\begin{aligned} x(t) &= A_1(t) + D_1(t) \\ &= A_2(t) + D_2(t) + D_1(t) \\ &= A_3(t) + D_3(t) + D_2(t) + D_1(t) \end{aligned} \tag{17}$$

where $D_i(t)$ in W_{-i} is called details at decomposition level i after reconstructed from d_i and $A_i(t)$ in V_{-i} is called the approximation at decomposition level i after reconstructed from a_i. The down sampling with half frequency process keeps the decomposition moving on. Assume the sampling frequency of the original signal $x(t)$ is f, then $D_1(t)$ represents the detail in frequency band from $f/2$ to f, $D_2(t)$ represents the detail in frequency band from $f/4$ to $f/2$, $D_3(t)$ represents the detail in frequency band from $f/8$ to $f/4$, $A_3(t)$ represents the approximation in frequency band from 0 to $f/8$ respectively.

4.3 Mathematical Procedure of DTWS

The proposed DTWS method is based on the noisy signal model shown in (18).

$$g = x + qw \tag{18}$$

where g is the noisy HS signal, x is the clear HS signal without noises, w represents white noise with zero mean and unit variance, and q describes the noise intensity. In order to get a better idea of DTWS method, the detailed experimental results of HS signal with early aortic stenosis (EAS) disease from eGM benchmark database are given in Figure 14.

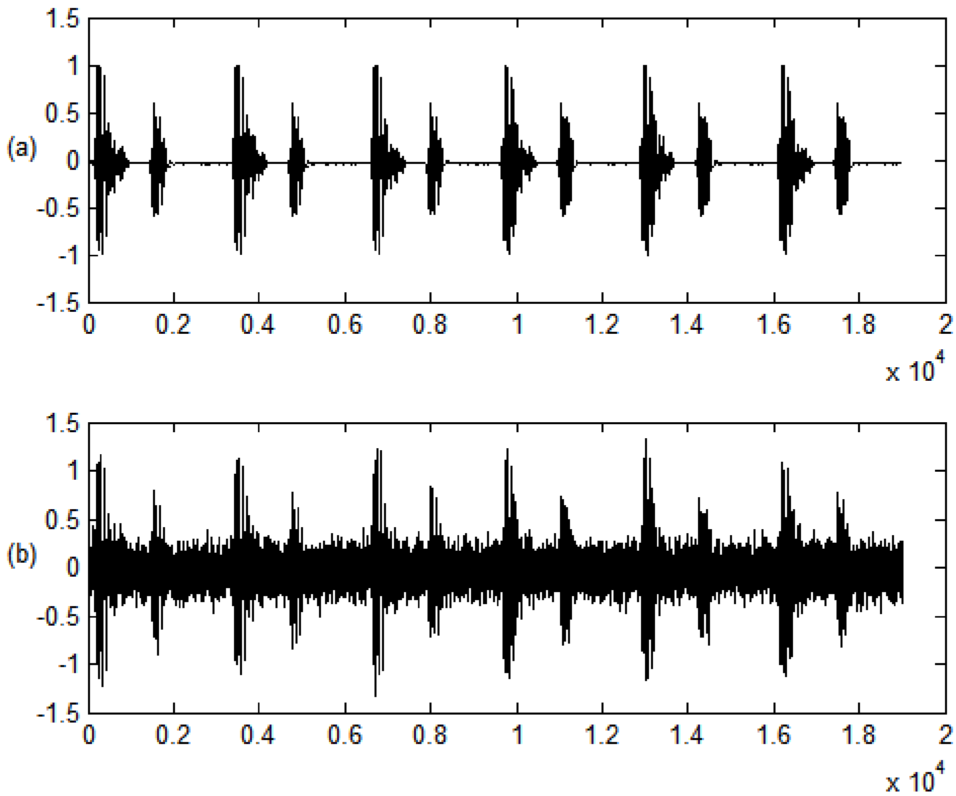

Figure 14: HS signal with EAS disease

The horizontal and vertical axes are amplitude and sample points respectively. The sampling frequency is 4000 Hz. Figure 14 (a) shows the original HS signal with EAS disease and white noises are added to the original signal which satisfies SNR = 5 dB is shown in Figure 14 (b) for further denoising and testing.

The mathematical procedure of proposed DTWS method is depicted in Figure 15. First, the input HS signal is decomposed using discrete wavelet transform to obtain wavelet coefficients of different layers. Based on these coefficients, the characteristic layers which contain most of the HS and murmurs information will be selected. After that, traditional shrinkage thresholds are applied on the non-characteristic layers while dynamic thresholds are performed on the characteristic layers thus to maintain the HS and murmurs information utmostly. Finally, the reconstructed HS signal is achieved through reconstruction from the wavelet coefficients of both characteristic and non-characteristic layers after shrinkage.

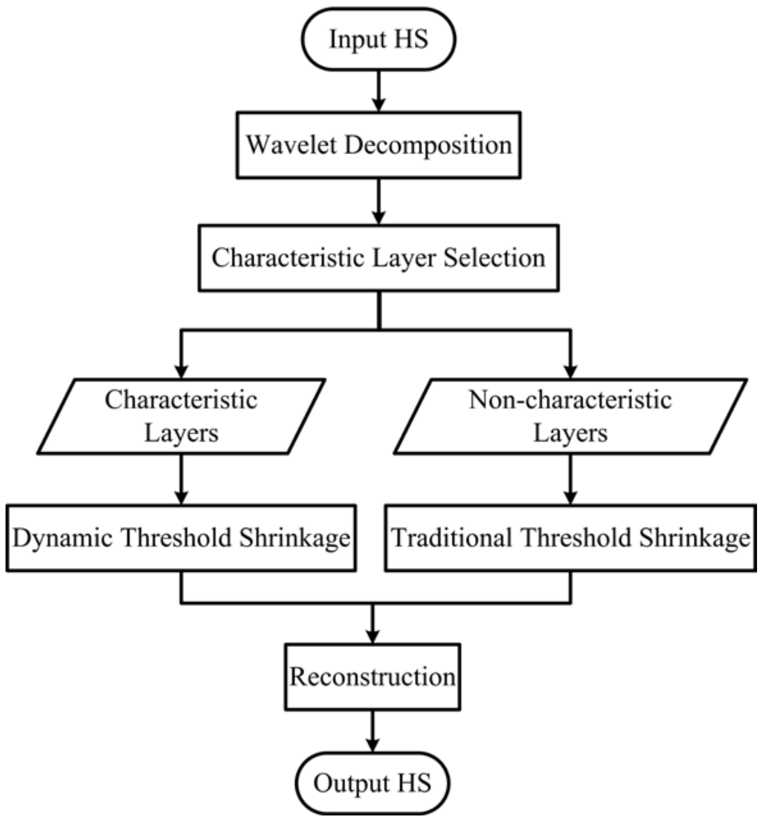

Figure 15: The mathematical procedure of proposed DTWS method

4.4 Decomposition

4.4.1 Mother Wavelet Selection

Daubechies (db) wavelet is a family of wavelet transforms discovered by Ingrid Daubechies. As the wavelet order increases, the order of vanishing moments increases correspondingly and makes the frequency band division result more clearly. The disadvantage is that real-time property will be worse. Considering the low time-varying characteristic of HS signal, applying high-order db wavelet is reasonable. After groups of simulations, db20 wavelet is chosen as the mother wavelet for wavelet decomposition.

4.4.2 Decomposition Level Selection

For quantitative measurement and comparisons, SNR and RMSE are used to evaluate the denoising performance as defined in Eq. (19) and Eq. (20) respectively.

$$\mathrm{SNR} = 10 \times \lg\{\sum_{n=1}^{l} x^2(n) / \sum_{n=1}^{l} [x(n) - \hat{x}(n)]^2)\} \tag{19}$$

$$\mathrm{RMSE} = \sqrt{\frac{1}{l}\sum_{n=1}^{l}[x(n) - \hat{x}(n)]^2} \tag{20}$$

where $x(n)$ represents the original clear HS signal without noises, $\hat{x}(n)$ is the reconstructed signal, and l is the signal length. Large SNR and small RMSE are desired for better denoising performance.

During DWT, the decomposition level L is very important for the following denoising since the smaller L leads to incomplete denoising whereas the larger L results in signal distortion. Tackling this, performance indicator SRR is defined in Eq. (21) as a quality factor for optimal L selection.

$$SRR = \frac{\mathrm{SNR}}{\mathrm{RMSE}} \tag{21}$$

It is obvious that, the maximal value of SRR corresponds to the optimal wavelet decomposition level L_{op}. Figure 16 illustrates the flowchart of optimal decomposition level selection. Initially, a default value L = 1 is employed in the first decomposition. After denoising using DTWS, *SRR* is calculated and recorded. Then, L increases by 1 and the next iteration starts to obtain the updated *SRR* value. The loop continues until L reaches the maximal value L_{max} which satisfies condition in Eq. (22).

$$\frac{f_s}{2^{L_{\max}}} > f_L > \frac{f_s}{2^{L_{\max}+1}} \tag{22}$$

where f_s is sampling frequency which is 4000 Hz in this HS sample and f_L is the minimum frequency of HS signals which is 20 Hz refer to the band-pass filter parameters in Chapter 3. Therefore, after all the iterations, the maximal *SRR* will be obtained thus the optimal decomposition level L_{op} can be achieved.

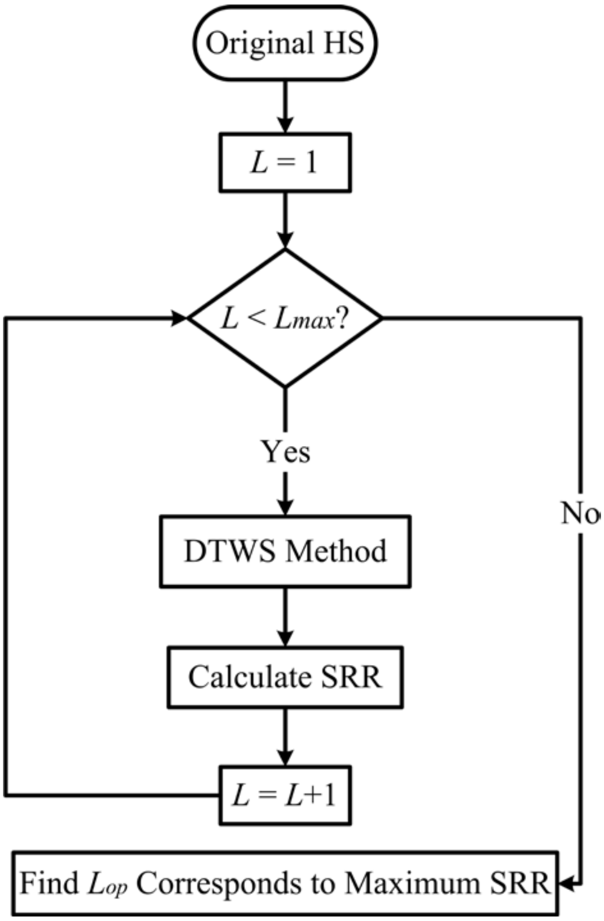

Figure 16: The flowchart of optimal decomposition level selection

In practical case, taking HS signal with EAS disease as an example. After adding white noise to original HS signal at the level of SNR = 5 dB, its performance indicator is calculated through the flowchart in Figure 16. The L_{max} is 8 as computed according to Eq. (22). The relationship between the value of *SRR* and decomposition levels is shown in Figure 17.

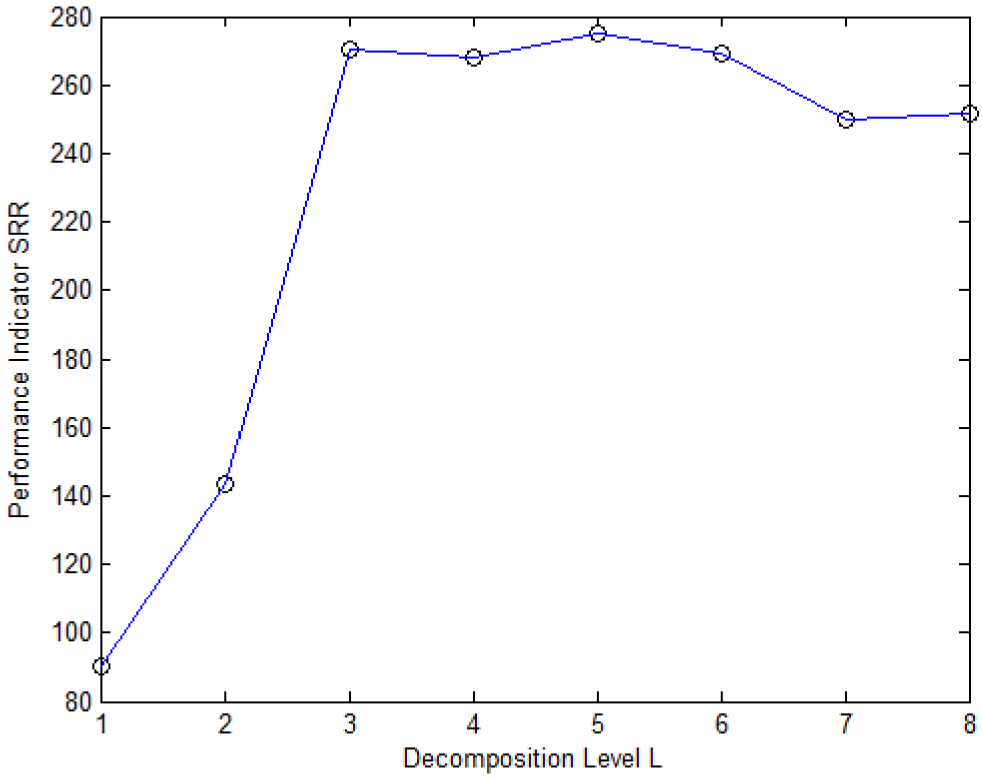

Figure 17: The relationship between *SRR* and decomposition level

It can be observed that decomposition at level 5 corresponds to the largest value of the performance indicator *SRR*. Therefore the optimal decomposition level is selected as 5 of the sample HS signal with EAS disease.

The decomposition results of details at each frequency band are shown in Figure 18, where Figure 18 (a) to (e) represents the details D_1 to D_5 at decomposition level 1 to 5 respectively.

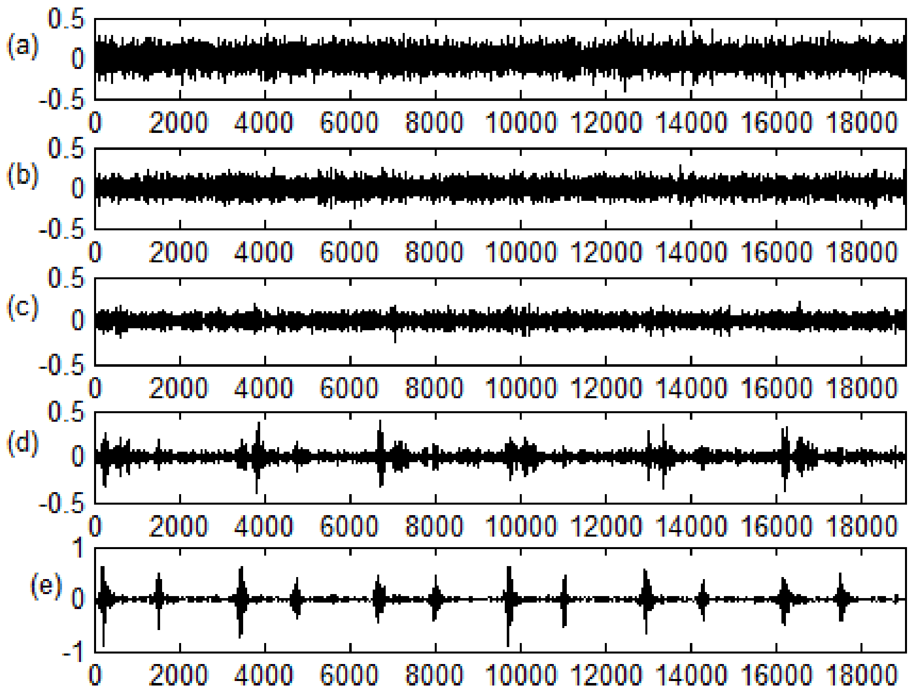

Figure 18: The decomposition results of details at each frequency band

4.5 Characteristic Layers Selection

Since murmurs exhibit comparable amplitudes with noises, a direct application of TWS method on the decomposed HS wavelet coefficients would cause over-shrinkage by mistaking murmurs as noises thus result in loss of murmurs information. Therefore, in order to eliminate the noises while keeping the pathological fidelity of murmurs simultaneously, the murmurs should be separated from noises before shrinkage. In this work, the wavelet decomposition layers containing most information of HS and murmurs with few noises are defined as characteristic layers, while layers containing most noises with few HS and murmurs information are defined as non-characteristic layers. Due to the periodicity difference between noises and HS or murmurs, the characteristic layers could be identified by calculating the autocorrelation of reconstructed signals in each wavelet decomposition layer as shown in Eq. (23).

$$r_j = \sum_{n=1}^{l-\eta} s_j(n) s_j(n+\eta) \tag{23}$$

where r_j and $s_j(n)$ are the autocorrelation result and reconstructed signal of jth decomposition layer respectively, l represents signal length, and η is the step length.

Figure 19 depicts the HS signal with EAS disease example about autocorrelation results. It is observed that the periodic signal exhibits periodic distribution symmetrically in the autocorrelation results (as shown in Figure 19 (a) to (c)), while for aperiodic signals the autocorrelation only shows peaks at the middle and both ends in the distribution axis (as shown in Figure 19 (d) and (e)). Therefore, the quasi-periodic property of HS components and murmurs makes it possible to differentiate the characteristic layers from the autocorrelation results of reconstructed signals in each decomposition layer.

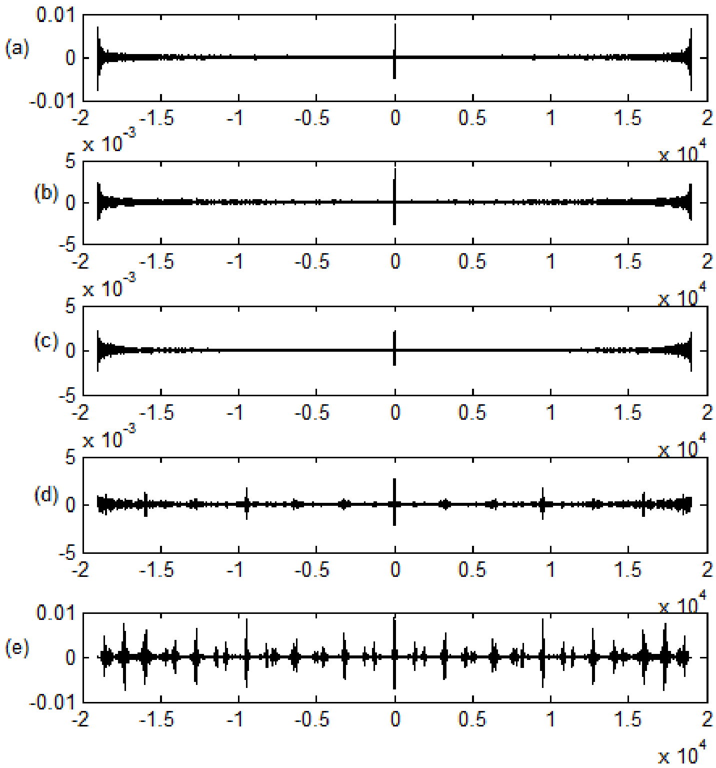

Figure 19: HS signal with EAS disease example about autocorrelation results

It can be found that (a) to (c) which correspond to details D_1 to D_3 at decomposition levels 1 to 3 are non-characteristic layers; (d) and (e) which represent details D_4 and D_5 at decomposition levels 4 and 5 are characteristic layers as defined previously.

4.6 Traditional Shrinkage on Non-Characteristic Layers

After identifying the characteristic layers and non-characteristic layers, different shrinkage thresholds are performed on wavelet coefficients of those layers for denoising. Since the characteristic layers mainly contain noises information, traditional shrinkage is performed on these layers.

Generally, the traditional shrinkage thresholds are set under four rules: sqtwolog, rigrsure, heursure, and minimax. In HS denoising, the heursure rule based heuristic threshold T_{heu} is proved to be optimal [15]. Different functions could be employed to conduct shrinkage based on the selected threshold, namely hard threshold function and soft threshold function as defined in (24) and (25) respectively.

$$y(c)=\begin{cases} c, & |c|\geq T_{heu} \\ 0, & |c|<T_{heu} \end{cases} \tag{24}$$

$$y(c)=\begin{cases} \operatorname{sgn}(c)\times(|c|-T_{heu}), & |c|\geq T_{heu} \\ 0, & |c|<T_{heu} \end{cases} \tag{25}$$

where c is the original wavelet coefficient, T_{heu} stands for the heuristic shrinkage threshold used in this work, and $y(c)$ describes the wavelet coefficient after shrinkage. In this work, the soft threshold function is employed for reason that the reconstructed signals become rough by using hard threshold function [14]. Through TWS method, noises in non-characteristic layers could be removed efficiently.

4.7 DTWS on Characteristic Layers

Differing from non-characteristic layers, the characteristic layers contain lots of HS and murmurs information. The pathological murmurs usually possess weak energy with low amplitudes in both time and frequency domain, thus are extremely sensitive to the shrinkage process. Hence, dynamic shrinkage thresholds are proposed for denoising of characteristic layers. Furthermore, the Shannon envelope technique based on normalized average Shannon energy [21] is employed before dynamic shrinkage, which could not only perform wavelet coefficients expression and suppression to increase the separation interval between noises and HS or murmurs, but also is beneficial for noises location during dynamic shrinkage. With the aid of a sliding window, the average Shannon energy could be calculated as defined in (26).

$$E_k=-\frac{1}{N}\sum_{m=1}^{N}W_{norm}^{2}(m)\log W_{norm}^{2}(m) \tag{26}$$

where E_k is the average Shannon energy of kth window, $W_{norm}(m)$ is the normalized wavelet coefficients within the window and N is window length. Subsequently, the normalized average Shannon energy of each window could be obtained:

$$P_k = \frac{E_k - \mathrm{Mean}(E_k)}{\mathrm{S\tan dard}(E_k)} \tag{27}$$

where P_k is the normalized average Shannon energy of kth window. After calculation, a series of Shannon energy could be achieved $\mathbf{P} = [P_1, ..., P_k, ..., P_N]$ is known as Shannon envelop of the wavelet coefficients. Afterwards, the dynamic threshold T_{dyn} in Eq. (28) is applied on the wavelet coefficients of characteristic layers based on the Shannon envelope.

$$T_{dyn} = \begin{cases} T_{heu}, & P_k \le TP \\ c_1 T_{heu}, & P_k > TP \end{cases} \tag{28}$$

where T_{heu} represents the aforementioned traditional shrinkage heuristic threshold, and TP is a fixed threshold utilized to identify noises and HS or murmurs as defined in Eq. (29), c_1 is an empirical coefficient.

$$TP = P_{min} + \frac{P_{max} - P_{min}}{c_2} \tag{29}$$

where P_{max} and P_{min} are the maximal and minimum value of Shannon envelope $\mathbf{P}$ respectively and c_2 is another empirical coefficient. It is observed that an envelope amplitude smaller than TP indicates noises, while an envelope amplitude larger than TP implies HS or murmurs. For instance, one of the characteristic layer's wavelet coefficients d_4 of the HS with EAS is shown in Figure 20 (a). The Shannon envelope of d_4 is represented by Figure 20 (b). The normalized Shannon envelope of d_4 and the fixed threshold TP is shown in Figure 20 (c).

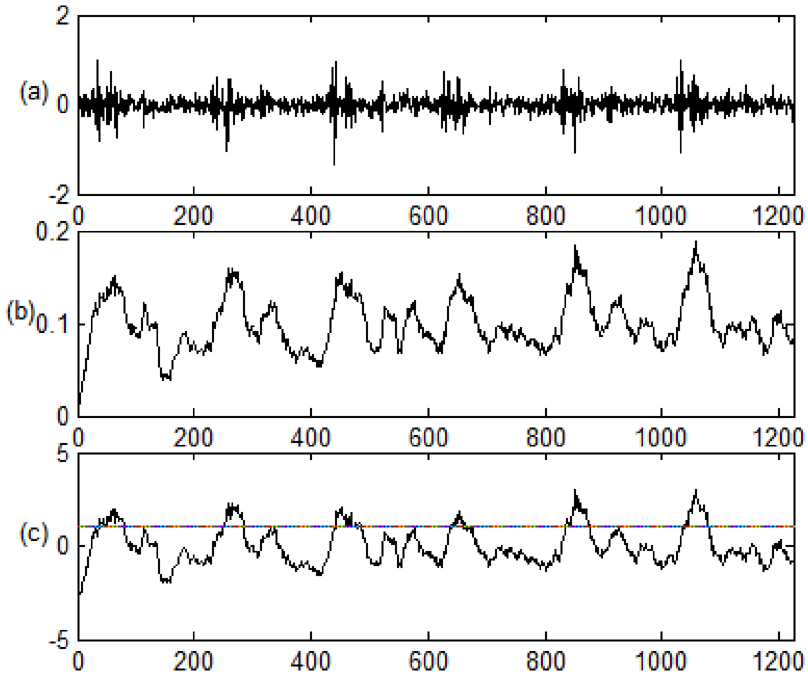

Figure 20. HS example of Shannon envelope and threshold setting

c_1 and c_2 are chosen to be 0.05 and 1.5 respectively as empirical coefficients in most of cases. The values of c_1 and c_2 can be adjusted after testing more HS signals.

Therefore, by conducting dynamic shrinkage on noises and HS or murmurs distinctly, DTWS could filter noises while retaining pathological fidelity of HS and murmurs properly. The dynamic threshold (red dash line) T_{dym} to d_4 at fourth layer of HS with EAS is shown in Figure 21 (a) as an example. And the result of shrinkage by the dynamic threshold is shown in Figure 21 (b).

4.8 Reconstruction

After applying different threshold on characteristic layers and non-characteristic layers, the renewed wavelet coefficients at each layer are reconstructed according to Eq. (16).

Finally, the reconstruction results of the HS with EAS example after denoising are obtained as illustrated in Figure 22, where (a) is the original HS with EAS signal without white noises, (b) is the reconstructed signal after DTWS denoising. For comparison usability, the denoising result of the same EAS signal by using TWS method is also plotted in (c). It is clearly seen that the pathological murmurs are well retained in (b), and in (c) the murmurs are distorted.

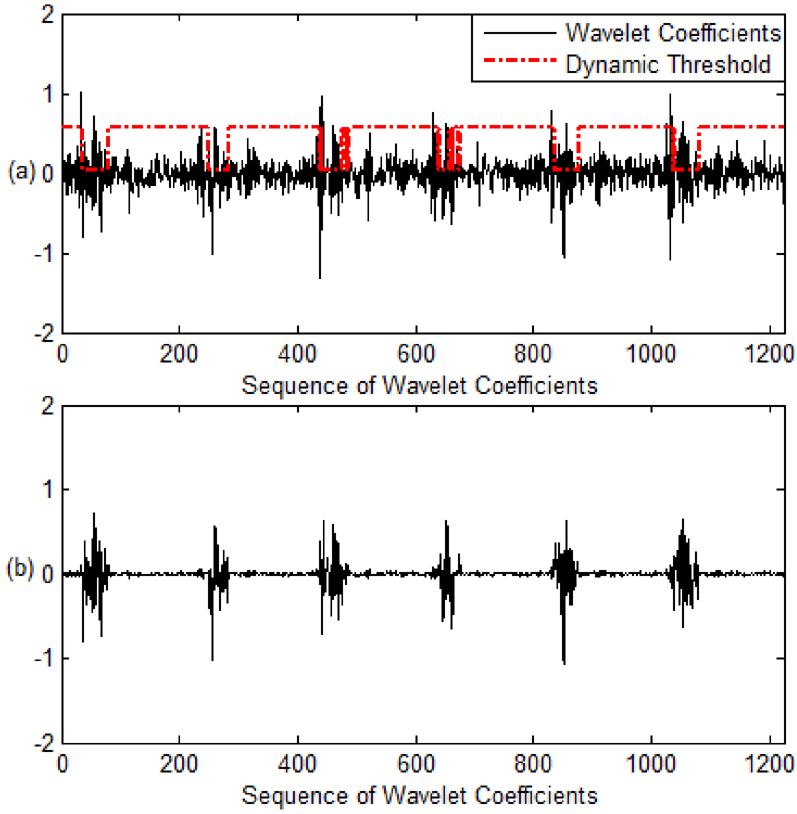

Figure 21: The dynamic threshold at one characteristic layer of HS with EAS

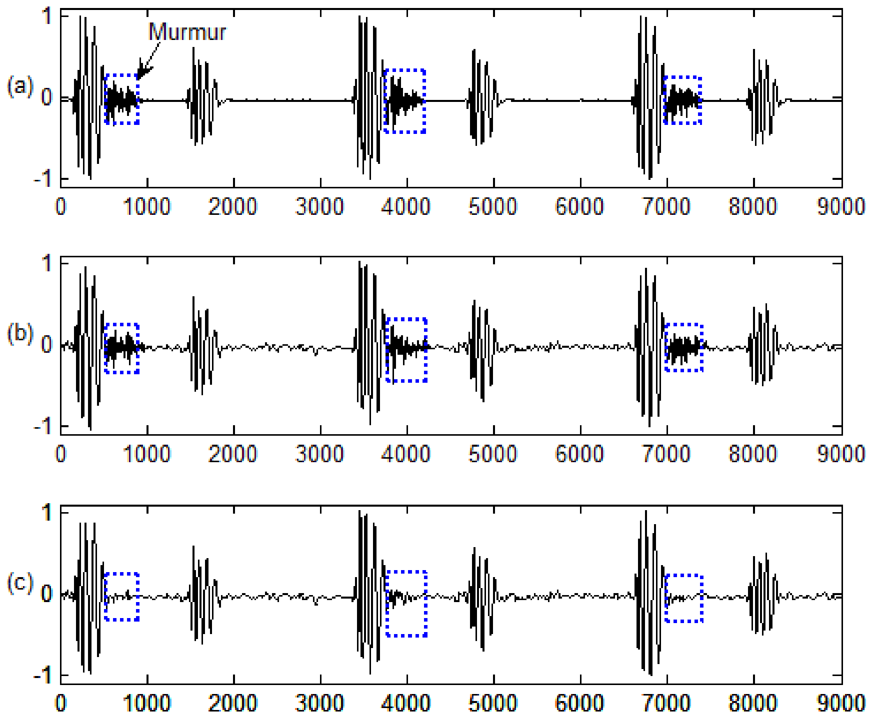

Figure 22: The reconstruction results of the HS with EAS example after denoising

CHAPTER 5: SINGULAR SPECTRUM ANALYSIS

In order to extract original heart sound signals from the noise, it is necessary to get the PC of the signal with noise. SSA is a powerful time series analysis technique which can extract the PC of HS signals. As the core of SSA, SVD utilizes the singular value spectra difference between HS signals and noise components. It is also effectively used for detection of murmur from HS signals.

In this work, the input HS signals of the SSA system are connected to the output of DTWS method. At this stage, the stationary noise (e.g. white noise) is eliminated from the original HS signals and the pathological information (murmurs) are retained simultaneously. However, there are some irregular external body noises such as environmental noises still exist in the HS signal, which may affect the accuracy of the subsequent analysis and diagnosis.

In this chapter, SSA is adapted in order to deal with the irregular noises (mainly environmental noises) mixed with the HS signals and satisfy the requirements of qualified HS signals for further analysis and diagnosis purposes.

The scheme of SSA is shown in Figure 23. There are mainly five steps to achieve SSA.

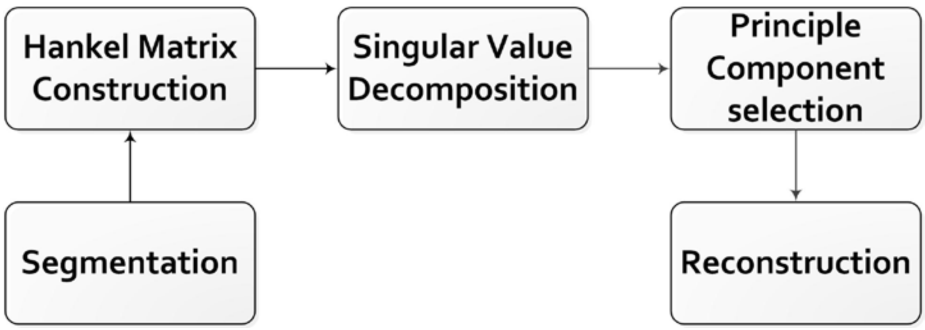

Figure 23: The scheme of SSA

5.1 Segmentation

Considering the fundamental calculation of SSA is matrix operation. The size of the trajectory matrix affects the computational complexity. Select the appropriate length for the SSA window results in good decomposition quality and low computational cost for the algorithm [12].

After denoising through DTWS method, HS signals are clear enough for segmentation directly. Utilizing the normalized Shannon envelope introduced in Chapter 4, the original HS signals can be segmented into several parts by cycles [6]. The schematic diagram of segmentation by normalized Shannon envelope is shown in Figure 24.

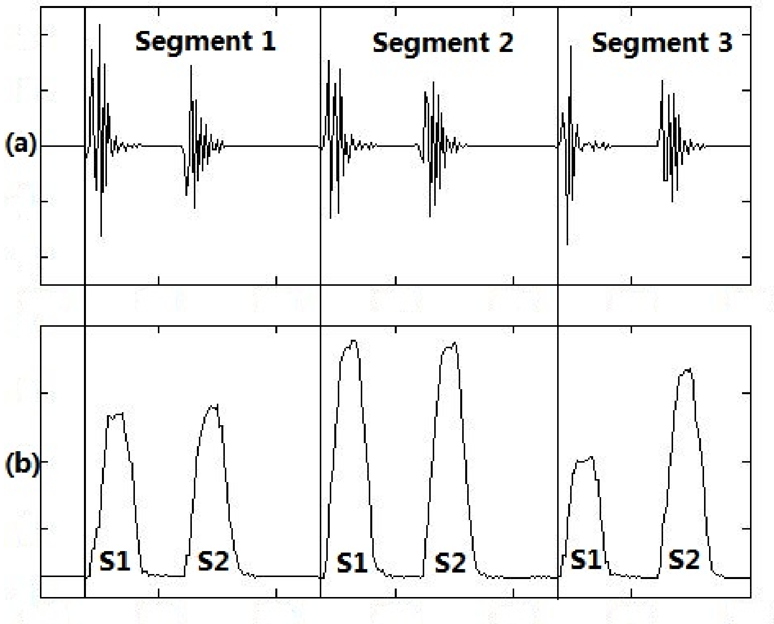

Figure 24: The schematic diagram of segmentation by normalized Shannon envelope

After obtaining the location information of S1 and S2, the HS signal can be segmented in cycles for further analysis. Each segment has the suitable window length *k* for SVD, which reserved in vector $\mathbf{S} = \{S_1, S_2, \cdots\cdots, S_N, \cdots\cdots, S_k\}$, where N indicates the sequence number of HS segments.

5.2 Trajectory Matrix Construction

Trajectory matrix construction is aim to transfer the one-dimension HS signals to the multi-dimension matrix. The trajectory matrix can be regarded as the trajectory of the HS signal sequence in embedding dimensions. The embedding dimension l is the most important parameter for trajectory matrix construction.

Cao's method mentioned in Chapter 2 provides means to determine the minimum embedding dimension from a time series. The greatest advantage of this approach is that it does not contain any subjective parameters except for the time-delay for the embedding. In the SSA of HS signals the time delay t is set to be unit through large quantity of tests, which is related to the sampling frequency of original HS signals. After obtaining the value of l and t, the Trajectory matrix can be constructed by Eq. (7).

The schematic diagram of trajectory matrix construction is shown in Figure 25.

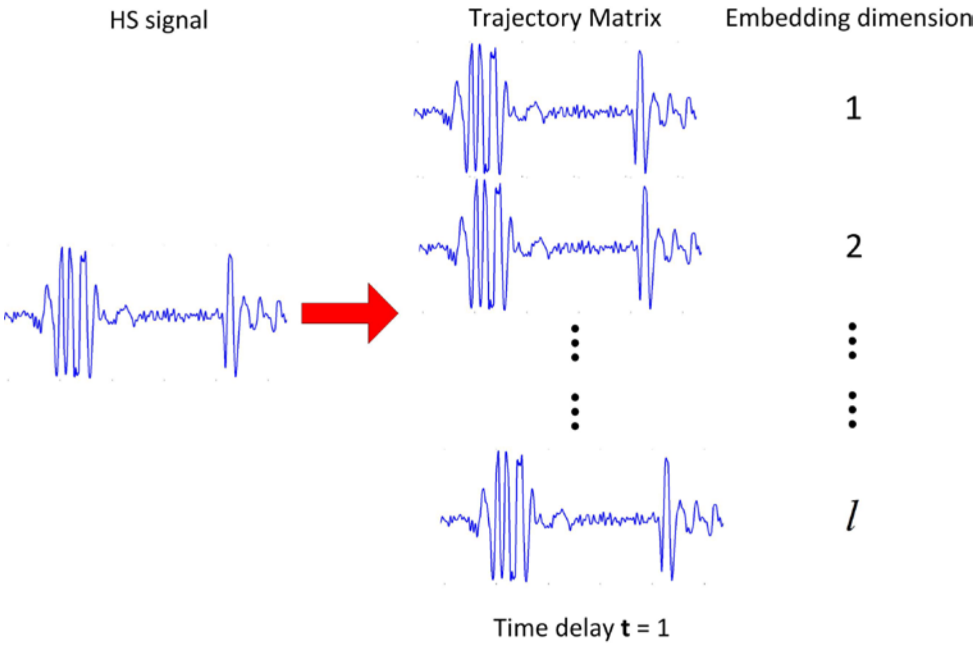

Figure 25: The schematic diagram of trajectory matrix construction

In Figure 25, l is the embedding dimension, which also is the number of rows of the trajectory matrix. The number of columns of the trajectory matrix equals to the total sampling points k of HS signal in one cycle. Finally the trajectory matrix is constructed as a $l \times k$ Hankel matrix called $\mathbf{X}$ as mentioned in Chapter 2.

5.3 Singular Value Decomposition

In linear algebra, the SVD is a factorization of a real or complex matrix, with many useful applications in signal processing and statistics. In this case, the trajectory matrix **X** constructed in section 5.2 can be considered as a factorization of the form:

$$\mathbf{X} = \mathbf{U}\sum\mathbf{V}^{*} \tag{30}$$

where **U** is a $l \times l$ real or complex unitary matrix, Σ depicts a $l \times k$ rectangular diagonal matrix with nonnegative real numbers on the diagonal, and V^{*} represents a $k \times k$ real or complex unitary matrix. The diagonal entries e_i of Σ are known as the eigenvalues of **X**. The l columns of **U** and the k columns of **V** are called the left-singular vectors and right-singular vectors of **X** respectively.

The schematic diagram of SVD is shown in Figure 26, where **E** is the diagonal entries vector of Σ, which is also known as eigenvector. The dash line indicates the dividing line of effective eigenvalues corresponds to PC of HS signal and non-effective eigenvalues corresponds to noise component of HS signal, which is also defined as "effective threshold".

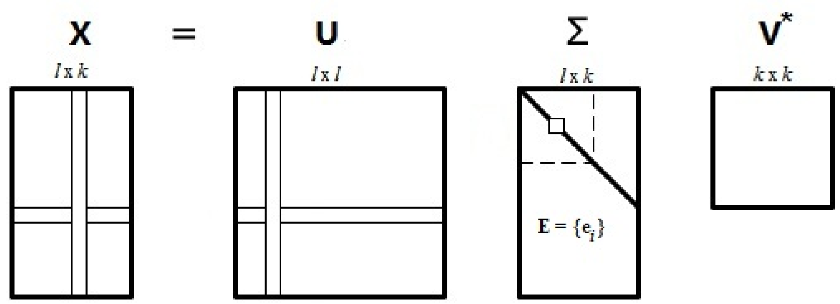

Figure 26: The schematic diagram of SVD

5.4 Principle Component Selection

In order to obtain the PC of HS signals, the effective eigenvalue selection from eigenvector **E** becomes a necessary process before reconstruction.

From larger quantity of simulations, it can be found that the curvature of the eigenvalues can be utilized to identify the PC and noise components of HS signals. The maximum curvature of the eigenvalues indicates the last effective eigenvalue, which is defined as σ corresponds to the location of effective threshold. A HS signal polluted by environmental noises with embedding dimension l = 20 is taken as an example to clarify the details of PC selection process. After SVD, the curve of eigenvalues e_i (i = 1, 2, ..., k) is shown in Figure 27:

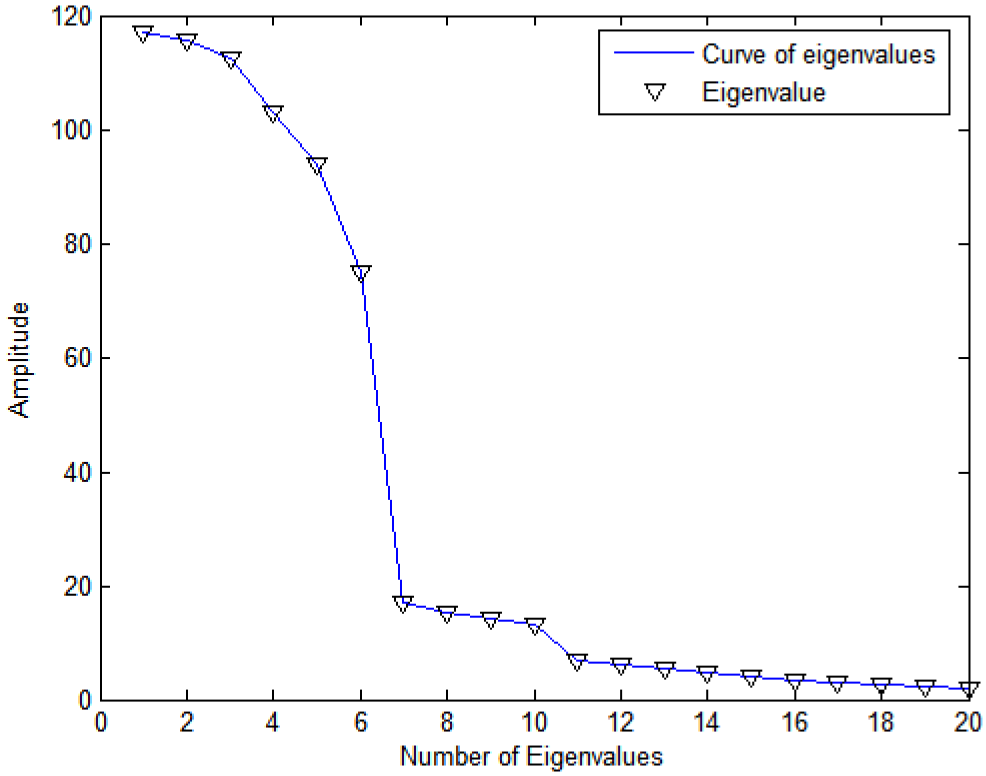

Figure 27: The curve of eigenvalues of the HS example

where the eigenvector of the HS signal **E** = {e_1, e_2, ..., e_{20}}. Since the eigenvalues are discrete points, the curvature of eigenvalues can be calculated by Eq. (32):

$$C_i = |e_{i+1} - e_i| \quad (i = 1, 2, \cdots, l-1) \tag{31}$$

where the lth curvature of eigenvalues is set to zero automatically. After calculating the curvature of eigenvalues, a new set named curvature vector **C** is generated. The curve of **C** is shown in Figure 28.

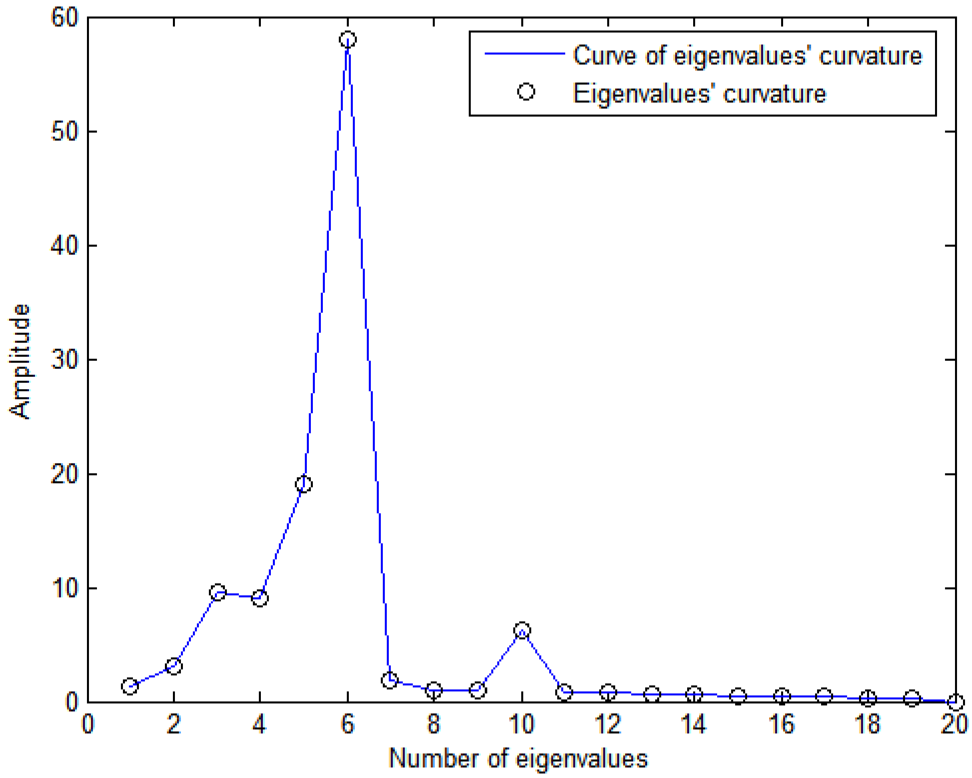

Figure 28: The curvatures of eigenvalue of the HS example

It can be observed that the maximum curvature value appears at 6^{th}, which indicates that the first six eigenvalues are effective eigenvalues, which corresponds to the PC of HS signal after reconstruction; while the remaining eigenvalues are non-effective eigenvalues, which corresponds to the noise components of HS signal after reconstruction. Referring to the illustration above, the effective eigenvalues are reserved and keep unchanged, whereas the non-effective eigenvalues are set to zero before reconstruction, which can be expressed by Eq. (33) as follows:

$$\mathrm{e}_i = \begin{cases} \mathrm{e}_i & 1 \le i \le \sigma \\ 0 & \sigma < i \le l \end{cases} \tag{33}$$

Figure 29 depicts the combination of the Figure 27 and Figure 28, it can be clear seen that the 6^{th} curvature of eigenvalues is the largest among curvature vector **C**, which indicates $\sigma = 6$. Figure 30 shows the adjusted eigenvalues Σ_{adj} before reconstruction.

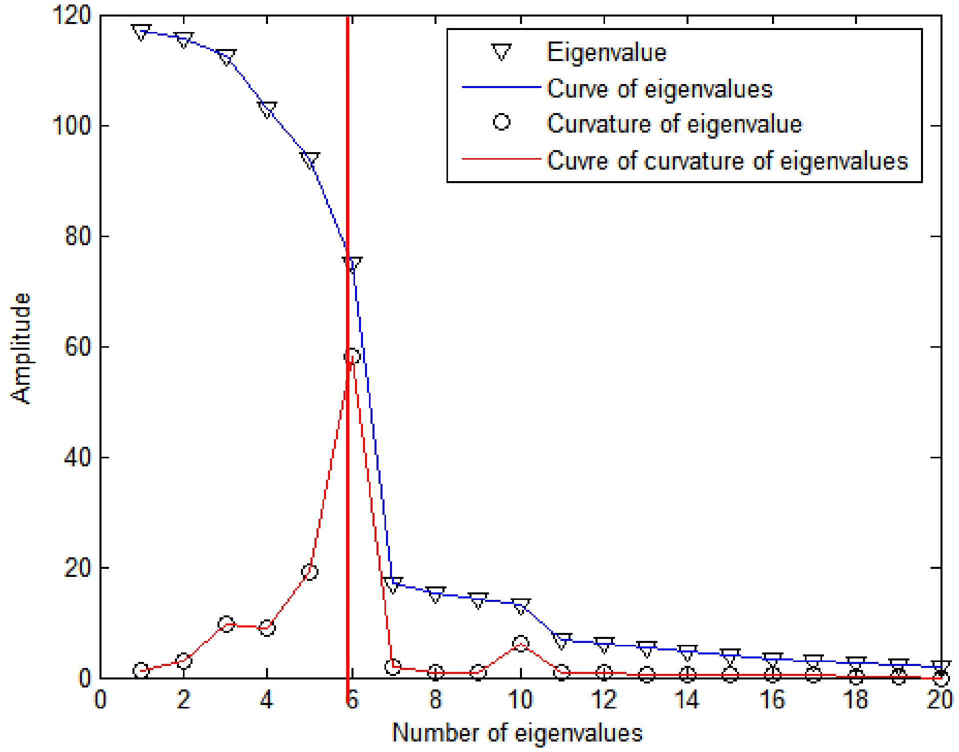

Figure 29: The curve and curvatures of eigenvalue of the HS sample

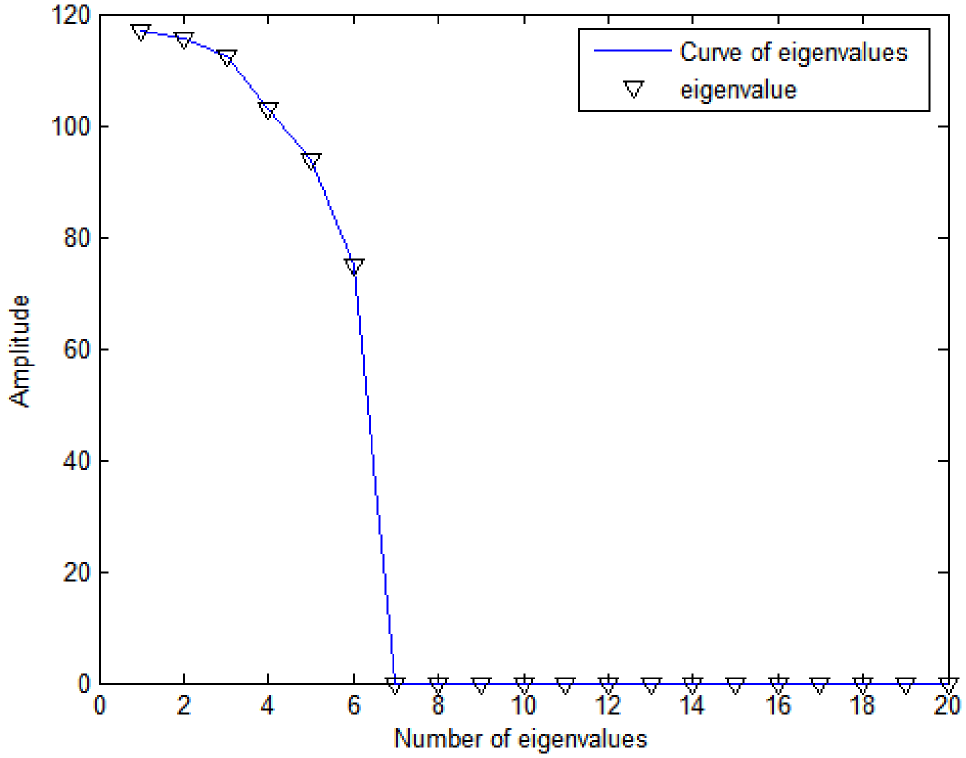

Figure 30: The adjusted eigenvalues before reconstruction

5.5 Reconstruction

After obtaining the adjusted eigenvalues Σ_{adj} by curvature of the eigenvalues, the reconstructed trajectory matrix $\mathbf{X}_{re}$ can be calculate by Eq. (34) as follows:

$$\mathbf{X}_{re} = \mathbf{U}\sum\nolimits_{adj}\mathbf{V}^{*} \tag{34}$$

where the unitary matrices $\mathbf{U}$ and $\mathbf{V}^{*}$ keep the same as the they are in decomposition results. The reconstructed heart sound signal can be derived by reduction dimension of the trajectory matrix $\mathbf{X}_{re}$ to one-dimension HS segments S_{Nre}, which is the inverse process of trajectory matrix construction introduced in section 5.2. Then the final reconstructed HS signal can be represent as a linear combination of HS segments in the reconstructed HS segments vector $\mathbf{S_{re}} = \{S_{1re}, S_{2re}, \cdots\cdots, S_{Nre}\}$. HS signal with S4 added with environmental noise is given as an example of SSA shown in Figure 31.

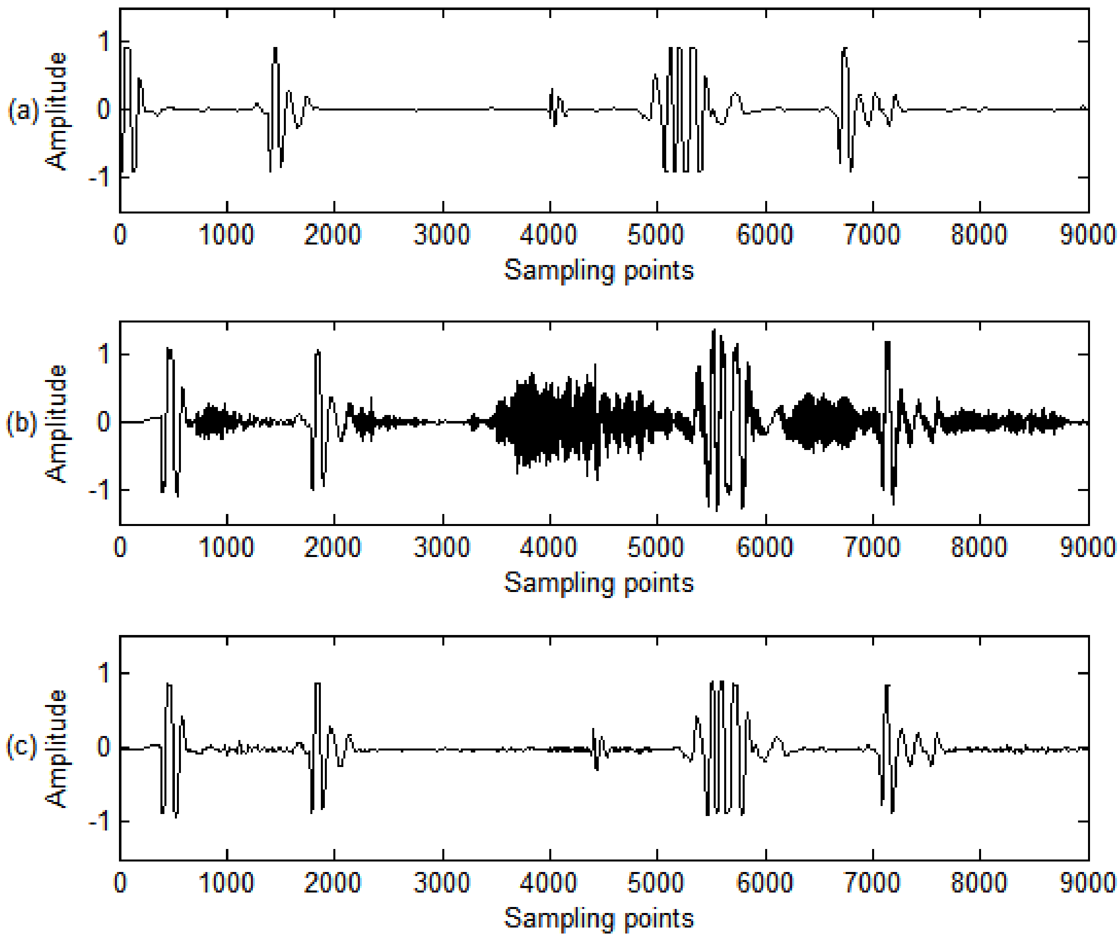

Figure 31: Denoising performance of HS signal with S4 added with environmental noise

where Figure 31 (a) is the original HS signal sample with S4 gallop. Figure 31 (b) is the superposition of the HS sample in Figure 31 (a) and random environmental noise collected from NOISEX-92 benchmark database. Figure 31 (c) is the reconstructed HS signal after SSA. The sight delay of de-noised result is caused by the band-pass filter in preprocessing part. It can be found that most of noise components are removed from the original HS signal and S4 gallop are retained as possible pathological information for further analysis and diagnosis.

As the reconstruction results of HS obtained, it is necessary to normalize the reconstructed signal by Eq. (11). The normalized signal can be regarded as the final output of the HS denoising system.

CHAPTER 6: TESTING AND EVALUATION

As introduced in chapters above, a HS denoising system is constructed as shown by the schematic diagram as follows:

Figure 32: The schematic diagram of HS denoising system

In order to verify the reliability and robustness of the HS denoising system, it is tested by empirical and clinical HS signals from different benchmark databases.

6.1 Source of Testing HS signals

HS benchmark database (4000Hz, 16-bit, 64kbps) provided by eGeneral Medical Inc., USA. (http://www.egeneralmedical.com/listohearmur.html)

NOISEX-92 environmental noise benchmark database (4000Hz, 16-bit, 64kbps) provided by Digital Signal Processing group, Rice University, USA. (http://spib.rice.edu/spib/select_noise.html)

HS segments of benchmark signals provided by Johns Hopkins University, USA.

HS segments of benchmark signals provided by University of Washington, USA.

HS signals measured from students and staffs at University of Macau.

The HSs and environmental noise samples mentioned above can be grouped into categories as follows:

TABLE II: HS AND ENVIRONMENTAL NOISE SAMPLES

Source	Number of HS samples
eGeneral Medical	17
Environmental Noise Database	37
Johns Hopkins University	6
University of Washington	16
Self-measured	7

6.2 Testing and Verification

In this section, four typical HS examples are presented for testing and verification of HS denoising system, which cover normal and abnormal HS with stationary and irregular noises respectively. The sampling frequency of HSs and environmental noises from eGeneral Medical benchmark database and Noisex-92 benchmark database are both 4000 Hz.

6.2.1 Normal HS with Stationary Noises

Figure 33 shows the denoising results of normal HS with stationary noises step by step.

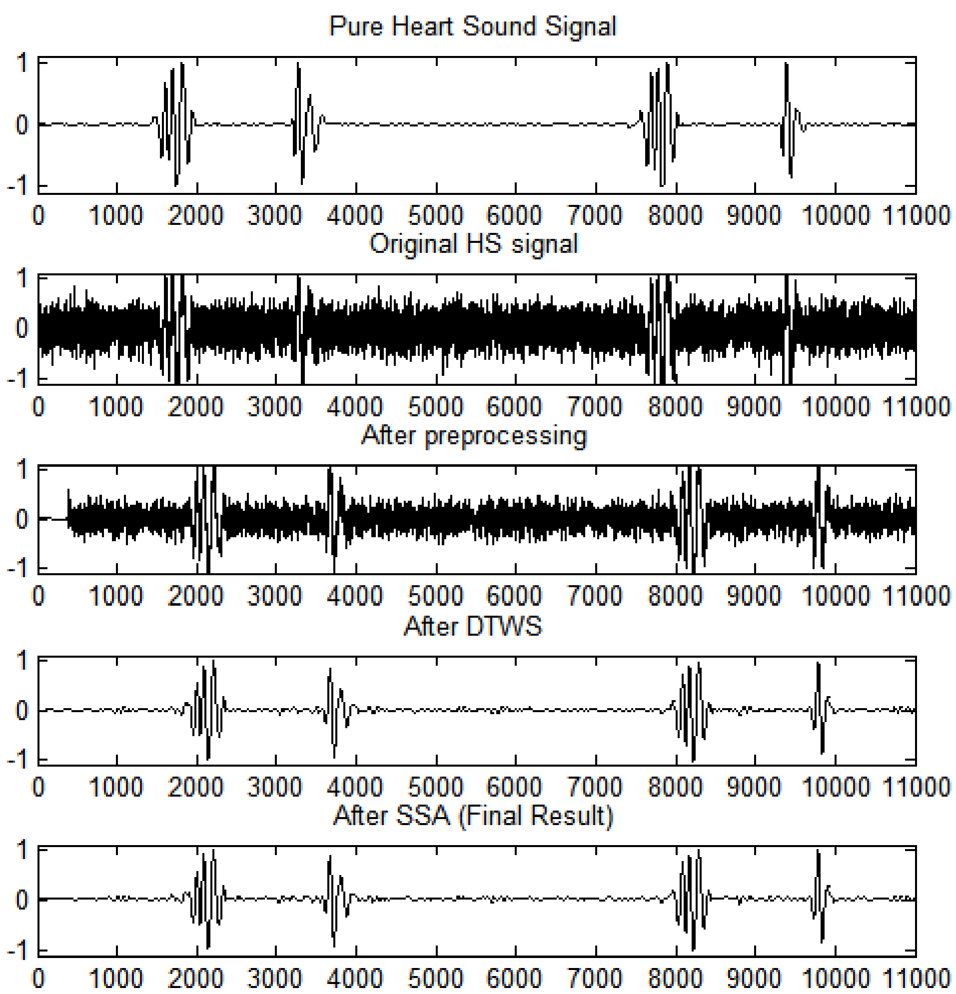

Figure 33: Denoising results of normal HS with stationary noises

The pure HS signal (normal HS) is from eGeneral Medical benchmark database, the original HS signal is normal HS added with white noise (stationary noise) which satisfies SNR = 0. Preprocessing part filters the noises out of the HS frequency band.

DTWS part eliminates the stationary noises, and SSA removes the irregular noises. In this case, since white noise is a kind of stationary noises, the HS signal after DTWS is qualified enough, SSA does not contribute too much on denoising.

6.2.2 Normal HS with Irregular Noises

Figure 34 shows the denoising results of normal HS with irregular noises step by step.

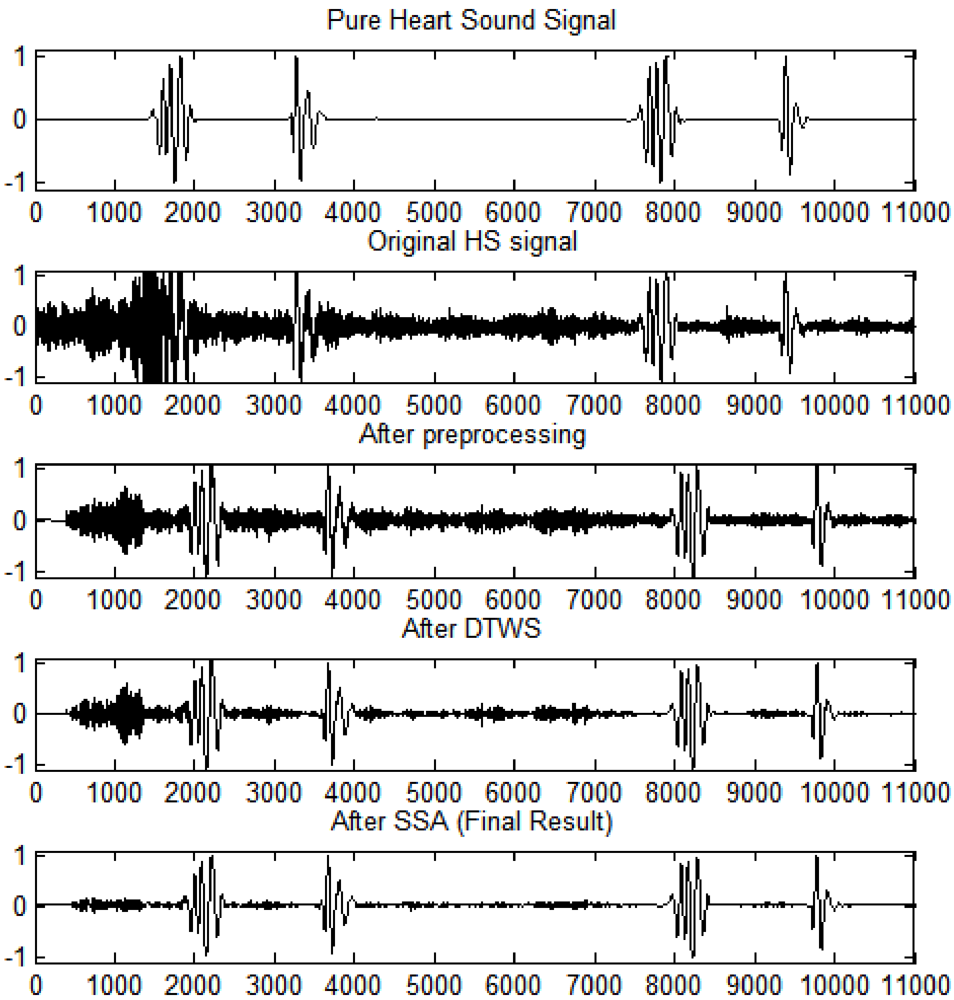

Figure 34: Denoising results of normal HS with irregular noises

The pure HS signal (normal HS) is still from eGeneral Medical benchmark database, the original HS signal is normal HS added with environmental noise collected from a kindergarten in NOISEX-92 environmental noise benchmark database (irregular noises), which satisfies SNR = 0. In this case, since environmental noise is a kind of irregular noises, DTWS does not contribute too much on denoising, while SSA plays an important role to eliminate the irregular environment noises.

6.2.3 Abnormal HS with Stationary Noises

Figure 35 shows the denoising results of abnormal HS with stationary noises step by step.

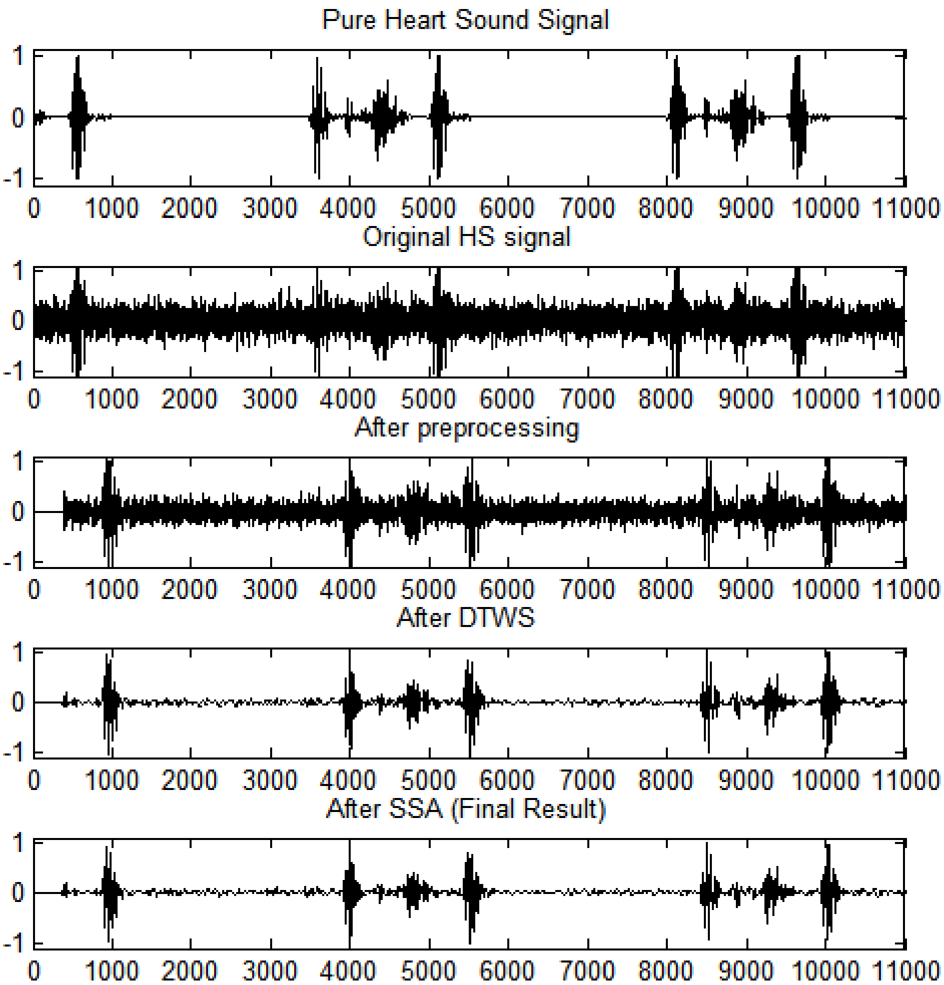

Figure 35: Denoising results of abnormal HS with stationary noises

The pure HS signal (abnormal HS) is mild aortic stenosis (MAS) from eGeneral Medical benchmark database, the original HS signal is abnormal HS added with white noise (stationary noises) satisfies SNR = 0. In this case, since white noise is a kind of stationary noises, the HS signal after DTWS is qualified enough, the stationary white noise is eliminated and murmur information between S1 and S2 are retained. SSA does not contribute too much on denoising.

6.2.4 Abnormal HS with Irregular Noises

Figure 36 shows the denoising results of abnormal HS with irregular noises step by step.

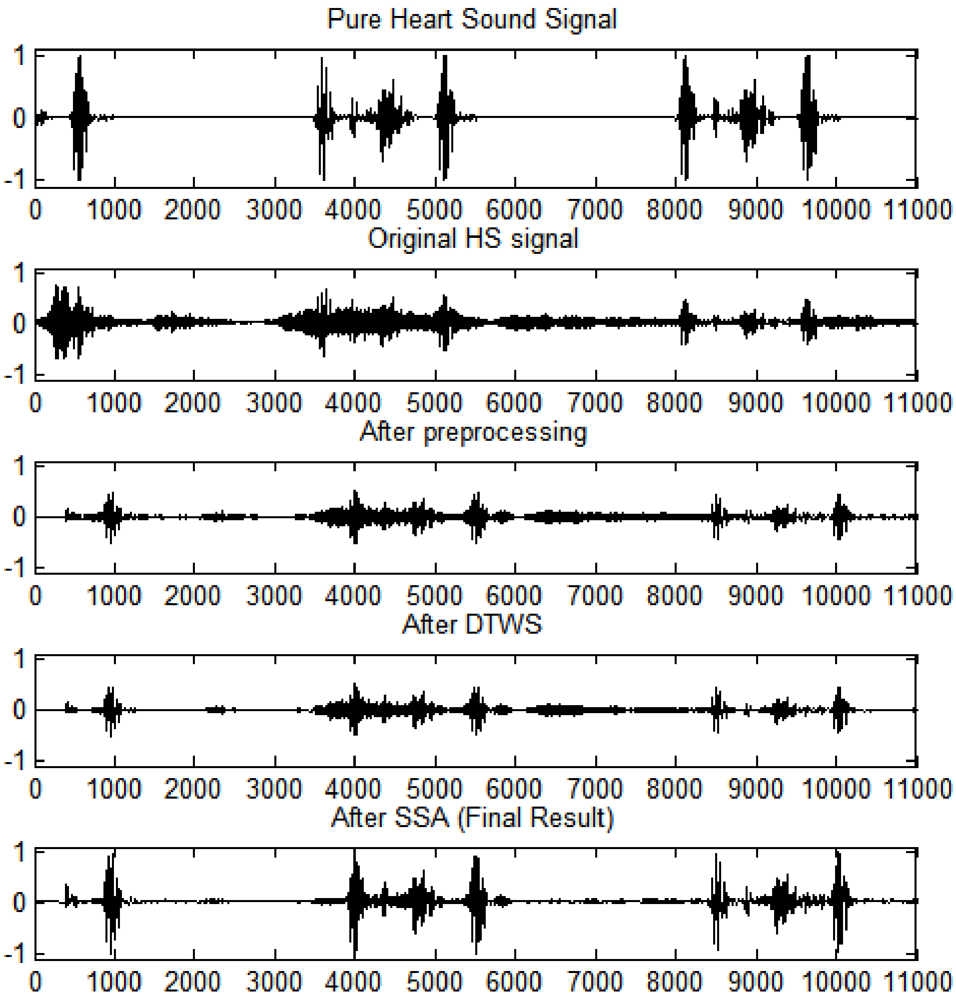

Figure 36: Denoising results of abnormal HS with irregular noises

The pure HS signal (abnormal HS) is MAS from eGeneral Medical benchmark database, the original HS signal is abnormal HS added with environmental noise collected from a kindergarten in NOISEX-92 environmental noise benchmark database (irregular noises), which satisfies SNR = 0. In this case, since environmental noise is a kind of irregular noises, DTWS does not contribute too much on denoising, while SSA plays an important role to eliminate the irregular environment noises and retain the murmur information between S1 and S2.

6.3 Summary of Denoising Performance

As a summary of the HS denoising system performance constructed in this thesis, SNR and RMSE are used to evaluate the denoising performance as defined in Eq. (19) and Eq. (20) in Chapter 4 respectively. Groups of representative testing results are shown as follows in TABLE III and IV.

For the SNR (dB):

TABLE III: DENOISING PERFORMANCE BY SNR

HS/noise		Stationary noise	Irregular noise		
		White	Traffic	Kindergarten	Human voice
Normal HS	eGM_nor	11.62	6.24	9.88	8.02
Abnormal HS	eGM_EAS	9.93	5.67	8.33	6.31
	eGM_MAS	10.12	5.41	8.46	6.59
	eGM_S4	11.14	6.29	9.76	7.83

For the RMSE (%):

TABLE IV: DENOISING PERFORMANCE BY RMSE

HS/noise		Stationary noise	Irregular noise		
		White	Traffic	Kindergarten	Human voice
Normal HS	eGM_nor	5.12	13.36	3.96	19.15
Abnormal HS	eGM_EAS	5.74	14.51	5.21	23.79
	eGM_MAS	5.36	14.75	4.83	21.60
	eGM_S4	5.33	13.55	4.01	19.64

where "eGM_nor", "eGM_EAS", "eGM_MAS" , and indicates eGM_S4 normal HS, HS with EAS disease, HS with MAS disease, and HS with S4 gallop respectively from eGeneral Medical benchmark databases. "Traffic", "kindergarten", and "Human voice" shows the environmental information correspondingly from NOISEX-92 environmental noise benchmark database. The original signal mixed with pure HSs and noises satisfied SNR = 0 dB.

From the testing results, the average SNR on normal HSs with stationary noises, normal HSs with irregular noises, abnormal HSs with stationary noises, and abnormal HSs with irregular noises are increased to 11.62, 8.05, 10.40, and 7.18 from 0 respectively. What's more, the low RMSE values of different combinations by HS and noise indicates the similarity between de-noised signals and pure HS signals from benchmark with high quality. As a conclusion, the HS denoising system proposed in the thesis has superior HS denoising performance to obtain qualified HS signals for further HS analysis and diagnosis purpose.

CHAPTER 7: CONCLUSION AND FUTURE WORK

E-home healthcare system provides a platform for HS analysis and diagnosis automatically. HS signal contains diversified pathological information and owns potential to monitor the health status of cardiovascular system, the possibility to provide early discovery and interposing makes it superior to clinical diagnosis after CVDs attacking.

As an important part of e-home healthcare system, a scheme of HS denoising system is proposed in this thesis. The input of HS denoising system is original HS signal collected from HS acquisition system and the output of system is the qualified HS signal for further HS analysis and diagnosis. The main research in this thesis is denoising method adapting DTWS and SSA. DTWS is based on the traditional wavelet shrinkage method, which utilizes a dynamic threshold to realize different shrink levels on noises and HS components by identifying them in characteristic layers. It overcomes the shortcomings of traditional wavelet shrinkage method and reserves the foremost HS and murmurs pathological information while eliminating stationary noises utmostly. SSA is implemented for irregular noises elimination by selecting the PC of HS according to the curvature of eigenvalues. The properties of zero phase-shift and without requiring prior information signal make it much more powerful in HS signal denoising. The test high-performances in denoising HS signals verify the reliability and efficiency of the proposed HS denoising methods.

Although the testing results show high performance of the proposed HS denoising methods, the HS denoising system scheme still needs further improvement to attach the optimal capability. Future works are expected by constructing professional HS database with more site-sampled HS recordings, which helps to adjust the parameters of threshold setting (e.g. TP, T_{heu}) thus to obtain the optimal empirical coefficients (c_1 and c_2) according to different kinds of CVDs through machine learning technique. Moreover, the qualified HS signals can be sent to HS analysis system for subsequent analysis. Comparing to analyzing the original HS signal directly, the improvement of CVDs diagnostic accuracy can be regarded as a more convincing indicator to evaluate the reliability and robustness of the proposed HS denoising methods.

BIBLIOGRAPHY

[1] A. Mertens., 1999. Signal Analysis: Wavelets, Filter Banks, Time-Frequency Transforms and Applications. John Wiley & Sons, Chichester, UK.

[2] Alwan A., 2011. Global status report on noncommunicable diseases 2010. World Health Organization.

[3] Blinowska, K. J. and Zygierewicz, J., 2011. Practical Biomedical Signal Analysis Using MATLAB®. CRC Press.

[4] Cao, L., 1997. “Practical method for determining the minimum embedding dimension of a scalar time series”. Physica D: Nonlinear Phenomena, Vol. 110, No. 1, pp. 43-50.

[5] Chan, T. F., Osher, S., & Shen, J., 2001. “The digital TV filter and nonlinear denoising”. IEEE Transactions on Image Processing, Vol. 10, No.2, pp. 231-241.

[6] Choi, S. and Jiang, Z., 2008. “Comparison of envelope extraction algorithms for cardiac sound signal segmentation”. Expert Systems with Applications, Vol. 34, No. 2, pp. 1056-1069.

[7] Djebbari, A. and Bereksi Reguig, F., 2000. “Short-time Fourier transform analysis of the phonocardiogram signal”. The 7th IEEE International Conference on Electronics, Circuits and Systems (ICECS), Vol. 2, pp. 844-847.

[8] Donoho, D. L. and Johnstone, J. M., 1994. “Ideal spatial adaptation by wavelet shrinkage”. Biometrika, Vol. 81, No. 3, pp. 425-455.

[9] Donoho, D. L., 1995. “De-noising by soft-thresholding”. IEEE Transactions on Information Theory, Vol. 41, No. 3, pp. 613-627.

[10] Fang-fang, B., Chang-yun, M., Cheng, Z., & Jing-meng, G., 2010. “Studying on denoising algorithm of heart sound signal based on the generalized mathematical morphology”. IEEE 10th International Conference on Signal Processing (ICSP), pp. 1797-1800.

[11] Fu, T. H., Liu, S. H., & Tang, K. T., 2008. “Heart rate extraction from photoplethysmogram waveform using wavelet multi-resolution analysis”. Journal of Medical and Biological Engineering, Vol. 28, No.4, pp. 229-232.

[12] Ghaderi, F., Mohseni, H. R., and Sanei, S., 2011. “Localizing heart sounds in respiratory signals using singular spectrum analysis”. IEEE Transactions on Biomedical Engineering, Vol. 58, No. 12, pp. 3360-3367.

[13] Gnitecki, J., Moussavi, Z., & Pasterkamp, H., 2003. “Recursive least squares adaptive noise cancellation filtering for heart sound reduction in lung sounds recordings”. Proceedings of the 25th Annual International Conference of the IEEE, Vol. 3, pp. 2416-2419.

[14] Han, M., Liu, Y., Xi, J., and Guo, W., 2007. “Noise smoothing for nonlinear time series using wavelet soft threshold”. IEEE Signal Processing Letters, Vol. 14, No. 1, pp. 62-65.

[15] Hong, Z., 2010. “Research and application of electric power signal filter based on wavelet multi-resolution technology”. IEEE International Conference on Environmental Science and Information Application Technology (ESIAT), Vol. 2, pp. 367-370.

[16] Hubbard, B. B., 1998. The World According to Wavelets: The Story of a Mathematical Technique in the Making. Universities Press.

[17] Kwak, C., & Kwon, O. W., 2012. “Cardiac disorder classification by heart sound signals using murmur likelihood and hidden Markov model state likelihood”. IET signal processing, Vol. 6, No.4, pp. 326-334.

[18] Martinez-Alajarin, J., & Ruiz-Merino, R., 2005. “Efficient method for events detection in phonocardiographic signals”. Microtechnologies for the New Millennium 2005, pp. 398-409.

[19] Mathers C.D. and Loncar D., 2006. “Projections of global mortality and burden of disease from 2002 to 2030”. PLoS Med, Vol. 3, No. 11, pp. 442.

[20] Messer, S. R., Agzarian, J., and Abbott, D., 2001. “Optimal wavelet denoising for phonocardiograms”. Microelectronics Journal, Vol. 32, No. 12, pp. 931-941.

[21] Meziani, F., Debbal, S. M., and Atbi, A., 2012. “Analysis of phonocardiogram signals using wavelet transform”. Journal of Medical Engineering & Technology, Vol. 36, No. 6, pp. 283-302.

[22] Misiti, M., Misiti, Y., Oppenheim, G., and Michel, J. P., 1996. Wavelet toolbox: for use with MATLAB. The MathWorks Inc, Natick, MA

[23] Rice, Mary J., et al, 1982. “Definitive diagnosis of truncus arteriosus by two-dimensional echocardiography”. The American Journal of Cardiology, Vol. 49, No. 4, pp. 1027.

[24] Sanei, S., Ghodsi, M., and Hassani, H., 2011. “An adaptive singular spectrum analysis approach to murmur detection from heart sounds”. Medical engineering & physics, Vol. 33, No. 3, pp. 362-367.

[25] Sreeram, N., Cheriex, E. C., Smeets, J. L., Gorgels, A. P., and Wellens, H. J., 1994. “Value of the 12-lead electrocardiogram at hospital admission in the diagnosis of pulmonary embolism”. The American journal of cardiology, Vol. 73, No. 4, pp. 298-303.

[26] Swanson, D., 2000. Signal Processing for Intelligent Sensor System, 1st ed., NewYork.

[27] Takens, F., 1981. “Detecting strange attractors in turbulence”. Dynamical systems and turbulence, Warwick 1980, pp. 366-381.

[28] Tilkian, A. G. and Conover, M. B., 2001. Understanding heart sounds and murmurs: with an introduction to lung sounds. WB Saunders.

[29] Varady, P., 2001. "Wavelet-based adaptive denoising of phonocardiographic records". Proceedings of the 23rd Annual International Conference of the IEEE, Vol. 2, pp. 1846-1849.

[30] Wang, Y., Wang, H. B., and Liu, L. H., 2010. "Noise reduction for heart sound based on wavelet transform". Information and Electronic Engineering, Vol. 8, No. 3, pp. 303-307.

[31] Xiali, Z., 2013. "An Exploration of Heart Sound Intelligent Interpretation Using MRA-Envelogram Cooperated MFCC Feature Extraction and DTW Classification". Master's thesis, University of Macau, Macau.

[32] Xiu-min, Z. and Gui-tao, C., 2009. "A novel de-noising method for heart sound signal using improved thresholding function in wavelet domain". IEEE International Conference on Future, pp. 65-68.

[33] Yoganathan, Ajit P., et al., 1976. "Use of the fast Fourier transform for frequency analysis of the first heart sound in normal man". Medical and biological engineering, Vol. 14, No. 1, pp. 69-73.

[34] Zhao, Z. D., 2005. "Wavelet shrinkage denoising by generalized threshold function". Proceedings of International Conference on Machine Learning and Cybernetics, Vol. 9, pp. 5501-5506.

APPENDIX: PUBLICATIONS

1. Tao ZENG, JiaLi MA, BinBin FU, and MingChui DONG, "An Exploration of Dynamic Threshold Wavelet Shrinkage Method for Heart Sound Denoising", accepted for publishing in the 3rd International Conference on Electronics Engineering and Informatics (ICEEI 2014), Bali, Indonesia, Sep. 2014. (Accepted on 13th of May 2014)

2. Tao ZENG, JiaLi MA, BinBin FU, and MingChui DONG, "Irregular Noise Elimination of Heart Sound Based on Singular Spectrum Analysis", to be submitted by the beginning of Jun. 2014.